DIRECTIONAL SOLIDIFICATION OF InSb-GaSb ALLOYS

N74 29898

By

James F. Yee, Sanghamitra Sen, Kalluri Samra,
Mu-Ching Lin and William R. Wilcox*
University of Southern California
Los Angeles, California 90007

SUMMARY

$In_xGa_{1-x}Sb$ with x = 0.5, 0.3 and 0.1 was directionally solidified under a variety of conditions. Identical gradient-freeze experiments were performed vertically with the heater on top, horizontally and in Skylab (SL-3). Experiments were also performed in SL-4 with the heater temperature increased. Bridgman-Stockbarger and vertical gradient freeze experiments were performed at USC. A transverse magnetic field was used to inhibit convection in some of the USC Bridgman experiments. A wide range of grain sizes was observed, but with no influence of growth conditions yet observed. The number of twins in the space-processed samples was much less than in the earth-processed samples. Equilibrium between the growing crystal and the bulk melt was more nearly achieved in the horizontally processed ingot, because of the enhanced free convection. Gas bubbles were trapped in the ingots when the ampoules were back-filled with helium. The bubbles were more evenly distributed in the Skylab ingots. Micro-cracks were more numerous in inhomogeneous regions of the ingots. The ingots formed in SL-3 had a smaller diameter than the tube, but those in SL-4 did not. The grains were very difficult to distinguish from one another in five out of six Skylab ingots.

*Paper presented by William R. Wilcox.

I. INTRODUCTION

Although a wide variety of semiconductor compounds are available, the selection of electronic and other physical property combinations is limited. The range of available property combinations becomes much larger if one considers solid solution alloys. For example, the electronic properties of InSb-GaSb alloys are such that Gunn microwave oscillation can be observed with some compositions, but not in pure InSb or GaSb (1). Unfortunately, large homogeneous single crystals of concentrated alloys are not produced. Films of many alloys can be produced by chemical vapor deposition or by liquid phase epitaxy, but many applications require bulk single crystals.

Directional solidification of concentrated alloy semiconductors produces a polycrystalline material. Homogeneous polycrystalline ingots may be produced by very slow zone leveling either with or without a solvent added, under conditions such that interface breakdown due to constitutional supercooling is avoided. One may speculate that grains are generated by the compositional variations arising from hydrodynamic fluctuations in the melt. In order to test this suggestion, directional solidification experiments were performed on InSb-GaSb alloys. These were carried out on the earth in vertical and horizontal positions, with and without a magnetic field, and in Skylab. While dramatic differences in grain size were not observed, several interesting phenomena were discovered.

II. SOLIDIFICATION EXPERIMENTS

The phase diagram for InSb and GaSb is shown in Figure 1. The conditions required to avoid constitutional supercooling were estimated from the phase diagram by use of the equation (3)

$$\left(\frac{G}{V}\right) > \frac{m}{D}\frac{C_c}{C_m}(X_c - X_m) , \qquad (1)$$

where G is the temperature gradient at the interface, V is the freezing

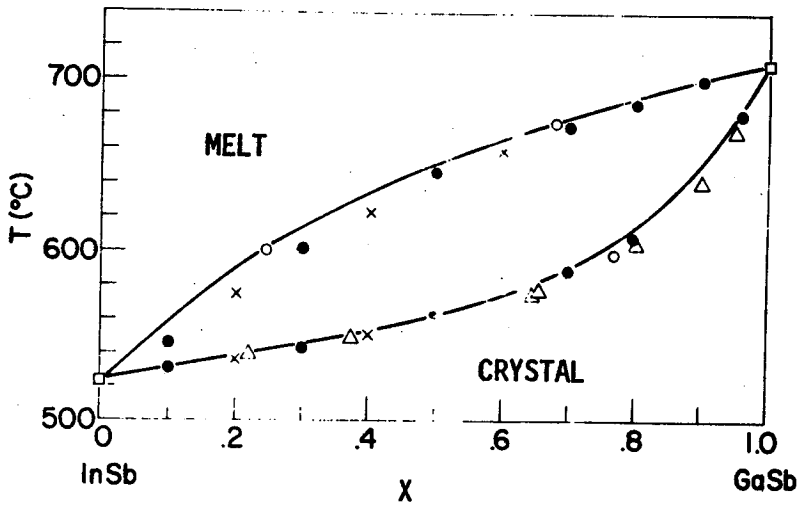

Figure 1. The InSb-GaSb pseudobinary phase diagram (2). X is mole fraction GaSb.

rate, m is the slope of the liquidus at the interfacial melt composition X_m, X_c is the mole fraction composition of the crystal, C_c is the total molar concentration in the crystal, C_m is the total molar concentration in the melt, and D is the binary diffusion coefficient (assumed to be 2×10^{-5} cm^2/sec). The results are shown in Figure 2. Conditions were chosen such that G/V was in the stable region at the beginning of solidification in each experiment. Mixtures initially containing 10%, 30% and 50% InSb were employed.

A. NASA Experiments

For the NASA earth and SL-3 experiments the value of G/V at the beginning of resolidification was estimated by use of heat transfer calculations (performed by Westinghouse (6)) to have been 816°C hour/cm^2. For SL-4 processed ingots the initial G/V was similarly estimated to have been 866°C hour/cm^2.

Fused silica tubing of 8 mm nominal inside diameter and 1 mm wall thickness was cut into nine-inch lengths and sealed at one end to prepare them for casting. Each such tube was cleaned in soap and water, followed by aqua regia and a rinse in semiconductor grade

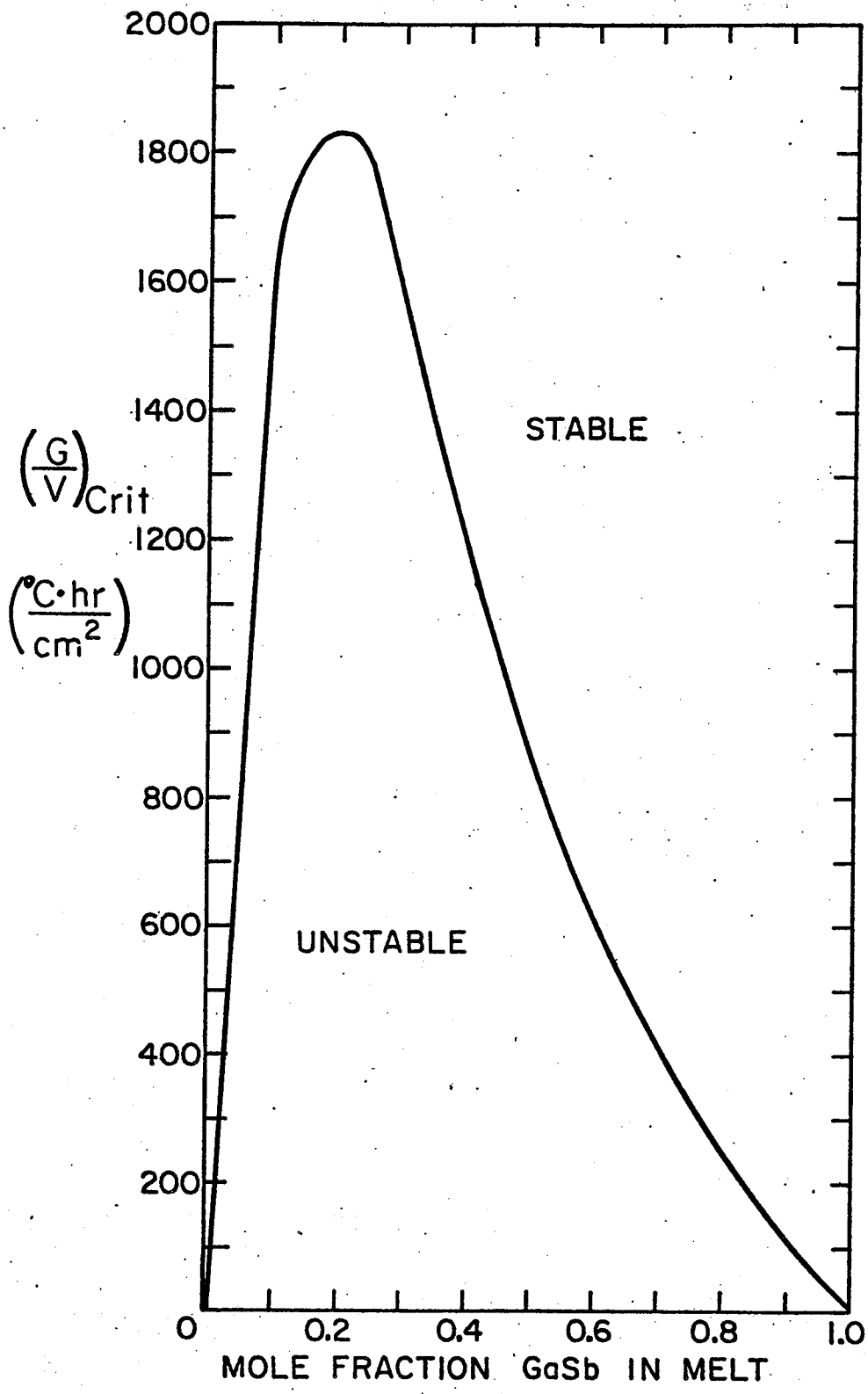

Figure 2. Critical G/V for constitutional supercooling in $In_xGa_{1-x}Sb$ calculated from Eq. (1).

deionized water. They were then heated in a horizontal furnace to over 920°C. Helium or argon was passed over acetone and into each capsule for a minimum of ten minutes, causing a layer of carbon to coat the interior walls of the capsule. The purpose of this coating was to prevent the sticking of the solid $In_xGa_{1-x}Sb$ to the walls of the silica capsule.

The elements were weighed in appropriate amounts and placed into the tubes. Each tube was sealed under a vacuum of less than 10^{-2} Torr. The ampoules were then heated in a vertical furnace at over 900°C for at least one hour. Frequent vigorous shaking was employed to enhance mixing of the melt. The ampoule usually cracked during cooling. Sometimes all of the silica could be mechanically removed quite easily from the ingot; sometimes it could not. In the latter case, HF was used to dissolve the quartz in one to two days. HF did not visibly attack the alloys in this period.

A typical cast ingot is shown in Figure 3. Longitudinal and cross-sectional slices of two $In_{0.3}Ga_{0.7}Sb$ ingots are shown in Figure 4. As can be seen, dendrites grew along the entire length of the ingot, as expected for such rapid solidification.

Each such ingot was cut to 9 cm length and chemically etched in 1 HNO_3:1 HCl in order to remove enough material at the surface so that it would fit loosely into carbon-coated 8 mm I.D. silica tubes. Graphite plugs, quartz wool and a small piece of silica tubing were used to encapsulate the sameles, as shown in Figure 5. The graphite plugs, made of high-purity Poco graphite DFP-2 rods (impurities < 5 ppm), were used as spacers to position the ingot and to confine the melt during crystal growth. The quartz wool was used as a spring to allow for the expansion of the ingot longitudinally during heating and crystal growth. The piece of quartz tubing was used to compress the assembly. The ampoules were evacuated and backfilled with 10 Torr of helium prior to sealing.

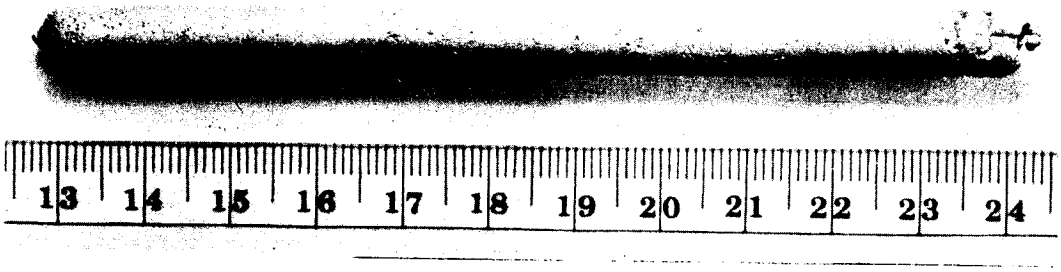

Figure 3. Photograph of casting.

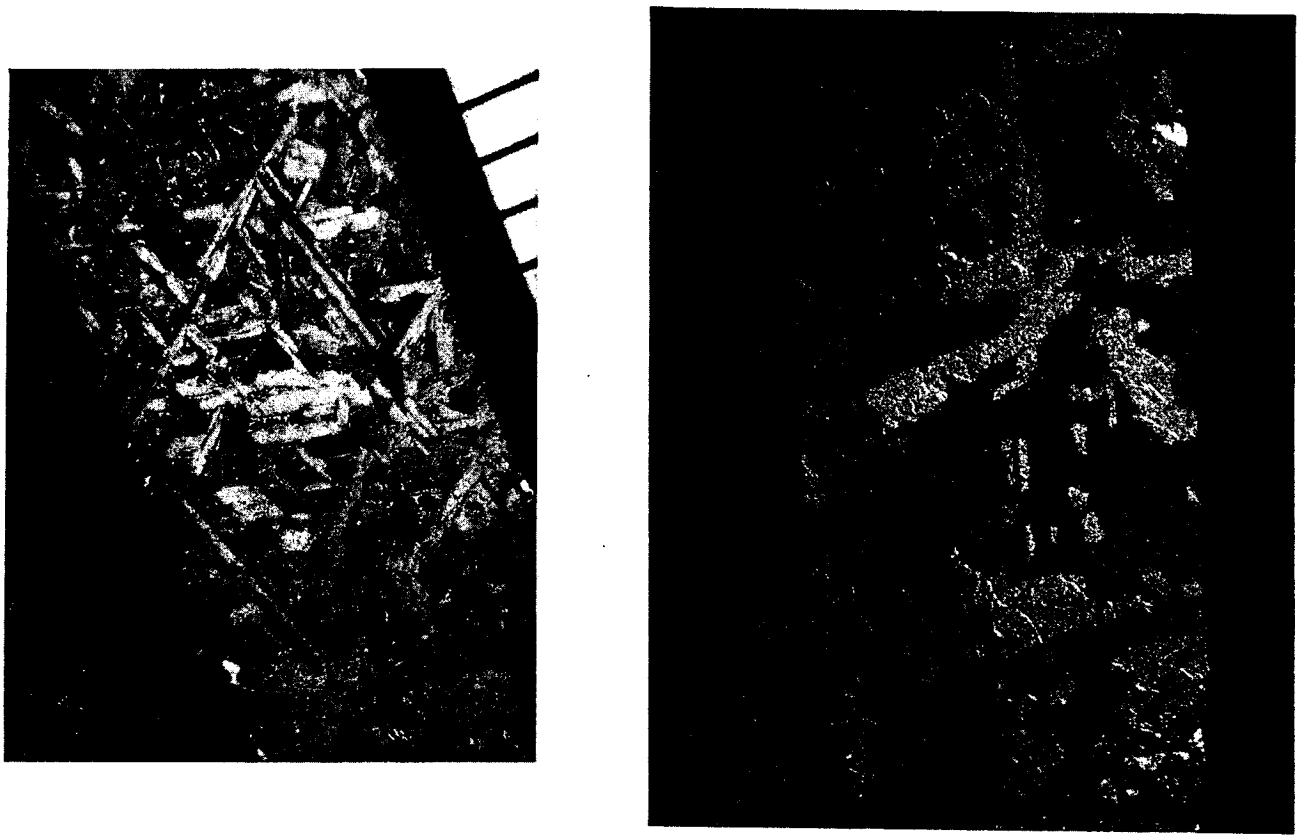

$In_{0.3}Ga_{0.7}Sb$ $In_{0.1}Ga_{0.9}Sb$

Figure 4. Photographs of cast ingots.

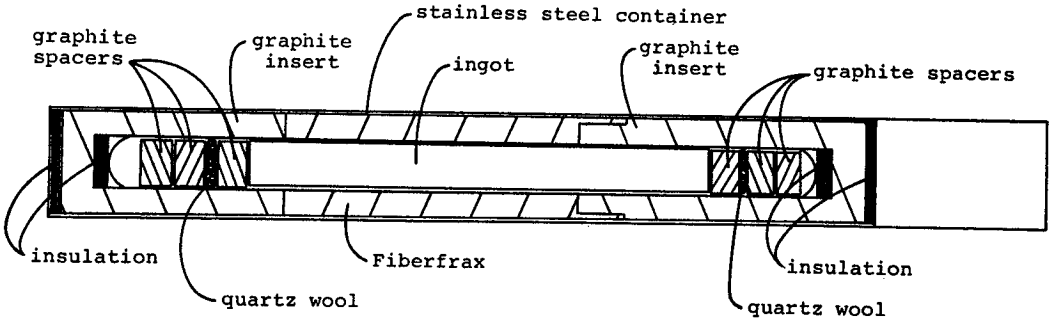

Figure 5. Diagram of completed ampoule in experimental cartridge.

These ampoules were then sealed by Westinghouse in stainless steel cartridges under a vacuum of $\leq 10^{-4}$ Torr. The cartridges were then processed by NASA in the Westinghouse Multipurpose Electric Furnace (6). This furnace consisted of a resistance heater at one end, a graphite heat extractor at the other, and an insulated region in between. Three cartridges were processed simultaneously in each run. As shown in Table I, three samples were processed vertically with the heater on top, three horizontally, three on the second Skylab mission, and three on the last Skylab mission. Power was applied so that the heater was at 960°C or 1020°C. This resulted in melting of somewhat over half of each ingot. After soaking for 16 hours to allow homogenization to occur, directional solidification was accomplished by programming down the heater temperature at 0.6°C per minute. This resulted in a steadily increasing freezing rate since the temperature gradient decreased as solidification proceeded. When the solid-liquid interface moved within the heater, the freezing rate increased rapidly because of the low temperature gradient there.

B. USC Experiments

Silica tubes of 9 mm I.D. were cleaned as before, but were not carbon coated because sticking and cracking were not a problem at the low solidification rates employed. Cleaner ingots with less oxides on their surfaces were obtained by etching the Sb and In shot in

TABLE I. SUMMARY OF NASA EXPERIMENTS

No.	Starting Composition	m.p. (°C)	Heater (°C)	Deviation from <111>	Length in Heater/Cooler[1]	Meltback x (cm)[2]
			Vertically Processed			
1A[3]	$In_{0.1}Ga_{0.9}Sb$	700	960		8.5/27.5 = 0.31	3.5
3B	$In_{0.3}Ga_{0.7}Sb$	678	960	18°	10.0/26/0 = 0.38	4.2
2C	$In_{0.1}Ga_{0.9}Db$	700	960	16°	12.0/24.0 = 0.50	3.7
			Horizontally Processed			
3A	$In_{0.5}Ga_{0.5}Sb$	646	960		9.5/26 5 = 0.36	4.6
4B	$In_{0.3}Ga_{0.7}Sb$	678	960	17°	14.0/22.0 = 0.64	4.6
4C	$In_{0.1}Ga_{0.9}Sb$	700	960	6°	8.5/27.5 = 0.31	4.0
			Skylab (SL-3) Processed			
2A	$In_{0.5}Ga_{0.5}Sb$	646	960		16.7/19.3 = 0.87	4.4
1B	$In_{0.3}Ga_{0.7}Sb$	678	960	9°	19.1/16.9 = 1.13	4.0
1C	$In_{0.1}Ga_{0.9}Sb$	700	960	9°	17.4/18.6 = 0.94	3.7
			Skylab (SL-4) Processed			
5A	$In_{0.5}Ga_{0.5}Sb$	646	1020		10.1/25.9 = 0.39	4.7
2B	$In_{0.3}Ga_{0.7}Sb$	678	1020		15.0/21.0 = 0.71	4.5
3C	$In_{0.1}Ga_{0.9}Sb$	700	1020		11.3/24.7 = 0.46	4.2

[1] In min.

[2] See Figure 13.

[3] Incorrectly labelled. Should have been 50% GaSb.

$1HC\ell:2H_2O$ for 10 to 15 minutes and then rinsing in methanol. The tubes were sealed under a vacuum of 5 to 10 x 10^{-3} Torr. An ampoule was then lowered into ~12 mm I.D. heater tube. The temperature was raised above the melting point of the desired alloy for 24 hours, with occasional shaking in order to produce a homogeneous melt.

Two different techniques were employed--the vertical Bridgman-Stockbarger technique and the vertical gradient freeze technique. Both furnaces were constructed by winding 22 gauge Kanthal wire on a grooved alundum furnace core. A diagram of the gradient-freeze apparatus is shown in Figure 6. The temperature gradient was produced by a cooled copper rod which projected 3 to 4 inches into the bottom of the furnace and contacted the ampoule. The heater tmperature was then slowly reduced by means of a temperature programmer. The initial value of G/V is estimated to have ranged from 300 to 500°C hour/cm^2.

A diagram of the Bridgman apparatus is shown in Figure 7. The voltage to the heater was held constant by a Sola constant voltage transformer in series with a variable autotransformer. The heater temperature was about 900°C, while the circulating coolant was at 4 to 5°C. The ampoule was lowered at 4 to 8 mm/day.

Temperature profiles in the Bridgman ampoule were measured by sealing a 5 mil chromel-alumel thermocouple in the tube. The thermocouple leads were in a two-holed alumina tube inside a silica tube. The alumina tube extended from the end of the silica tube. The thermocouple bead, formed at the end of the alumina tube, was coated with a ceramic cement to protect it from the melt. With the thermocouple fixed thereby, lowering the tube through the furnace produced the temperature profiles shown in Figure 8. The initial value of G/V in the growth experiments is estimated thereby to have been 930 to 1500°C hour/cm^2. The furnace profile in Figure 8 was measured by means of a thermocouple between an identical ampoule and the furnace tube wall.

Previous work on solidification of InSb in a horizontal boat showed that free convection could be greatly reduced by means of a

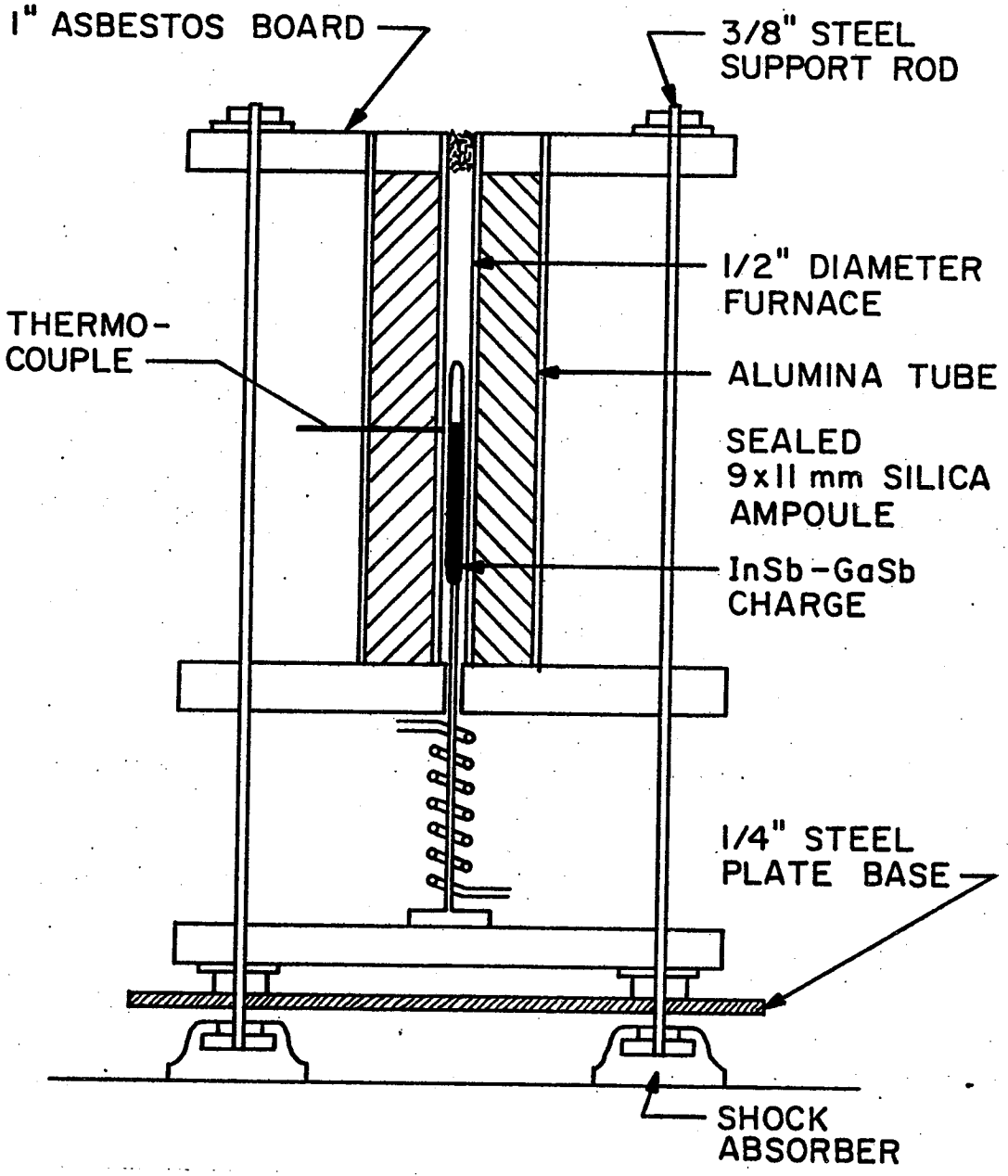

FIGURE 6. DIAGRAM OF GRADIENT-FREEZE APPARATUS FOR GROWTH OF $In_xGa_{1-x}Sb$.

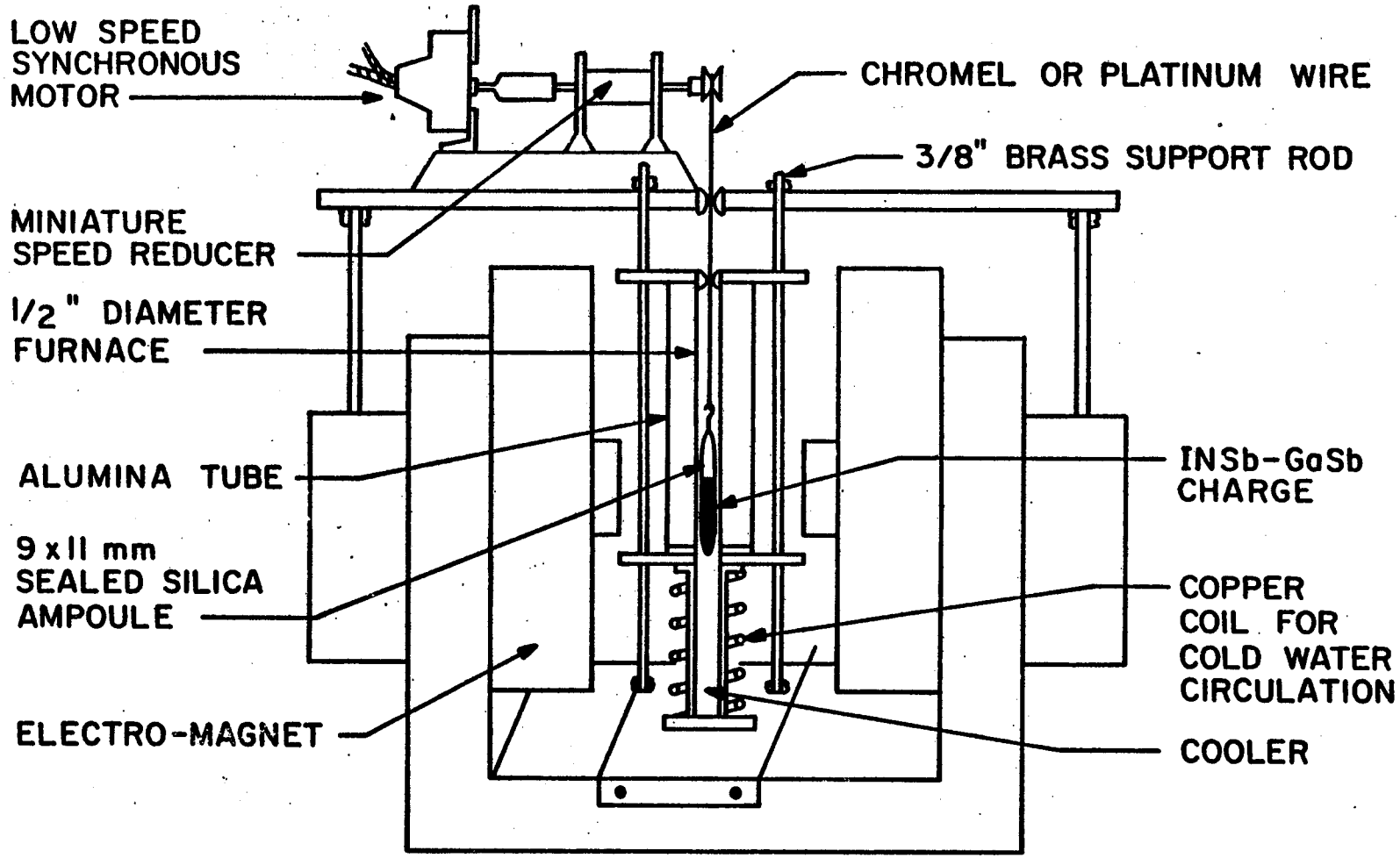

Figure 7. Diagram for vertical-Bridgman growth under magnetic field.

transverse magnetic field (4). We found that a transverse field in our Bridgman experiments altered the temperature profile as shown in Figure 9. This is indicative of reduced convection. No change in temperature distribution was noted as field strength was increased from 2 kilogauss to 4 kG, so 4 kG was used for the growth experiments. In several runs the field was turned on or off part way through the run.

III. RESULTS

A. Morphology

NASA provided X-radiographs of the unopened sampled cartridges after thermal processing, as shown in Figures 10-13. Note that the cross sections of the ingots processed horizontally were not circular. Those processed in SL-3 had irregular wavy surfaces with diameters somewhat less than the tube diameter. Ingot 1C had a diameter of only ~6.4 mm at one point. On the other hand, those ingots processed in SL-4 did have the tube diameter.

The radiographs, Figures 10-13, also allowed us to measure the melt-back position, as defined in Figure 14 and summarized in Table I. There was considerable variation in the amount of material initially melted in the thermal processing. There were two factors influencing the amount of melt-back: the thermal parameters of the semiconductor and the exact geometry of all components in the cartridge. The most important thermal parameter of the solid is its melting point, which increases as the gallium content increases. The lower the melting point, the more melt-back expected. The most important geometric factors are the length of solid in the heater and the length of solid in the cooler. The higher the ratio of the portion in the heater to that in the cooler, the more melt-back expected. If we examine Table I we see in comparing ingot 2C to 1A that the geometric effect was responsible for the larger melt-back. Comparing ingot 3B to 2C, the melting point effect predominated. The horizontally-processed ingots had appreciably more melt-back than the vertically-processed ingots.

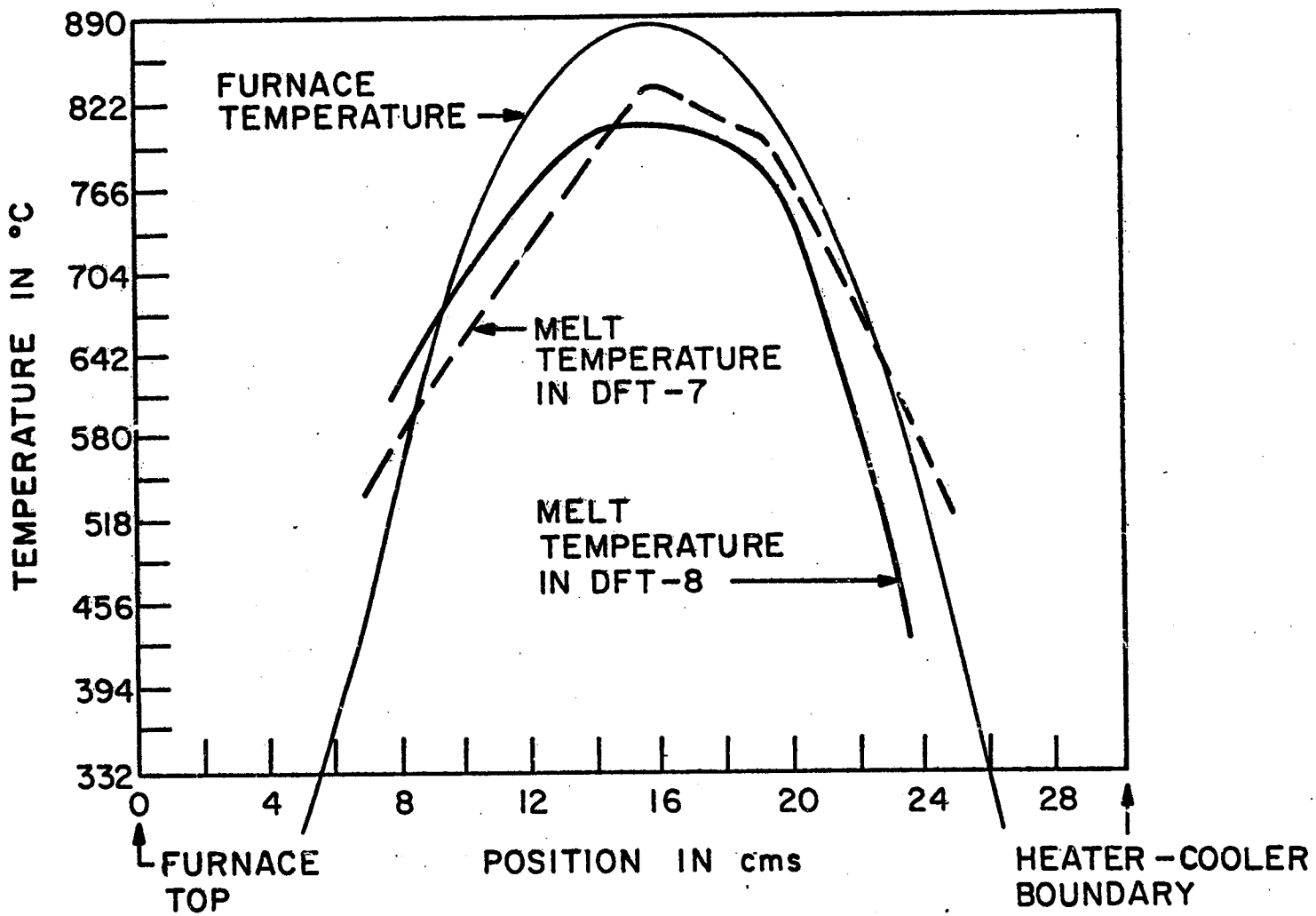

Figure 8. Measured temperature profile inside and outside vertical Bridgman growth ampoule (DFT-7 was $In_{0.1}Ga_{0.9}Sb$; DFT-8 was $In_{0.5}Ga_{0.5}Sb$).

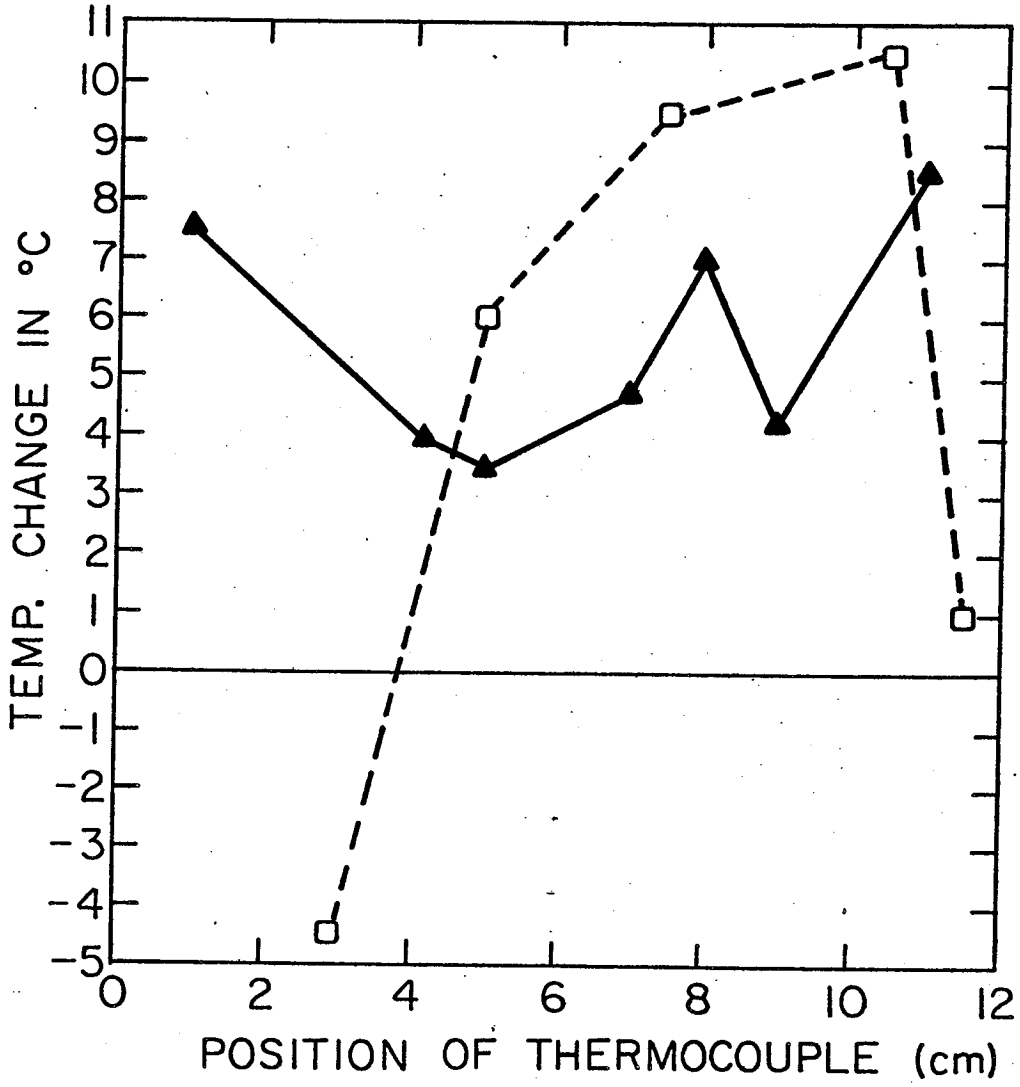

Figure 9. Change in temperature in Bridgman ampoule due to application of transverse magnetic field.

△ = DFT-8 ($In_{0.5}Ga_{0.5}Sb$)

□ - DFT-7 ($In_{0.1}Ga_{0.9}Sb$)

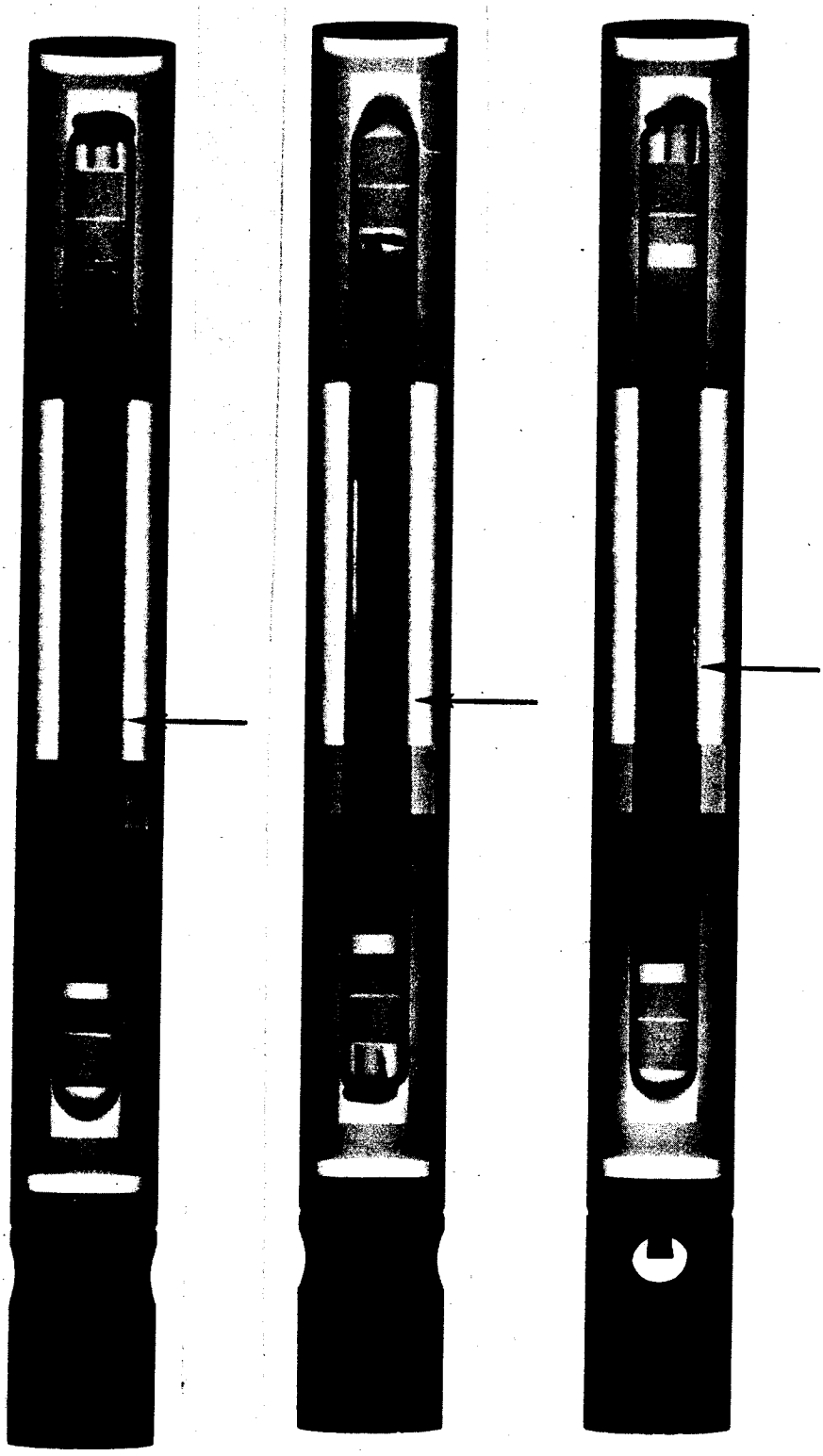

3A 4B 4C

Figure 10. X-ray images of cartridges processed on the ground in a horizontal position. Arrows indicate melt-back position.

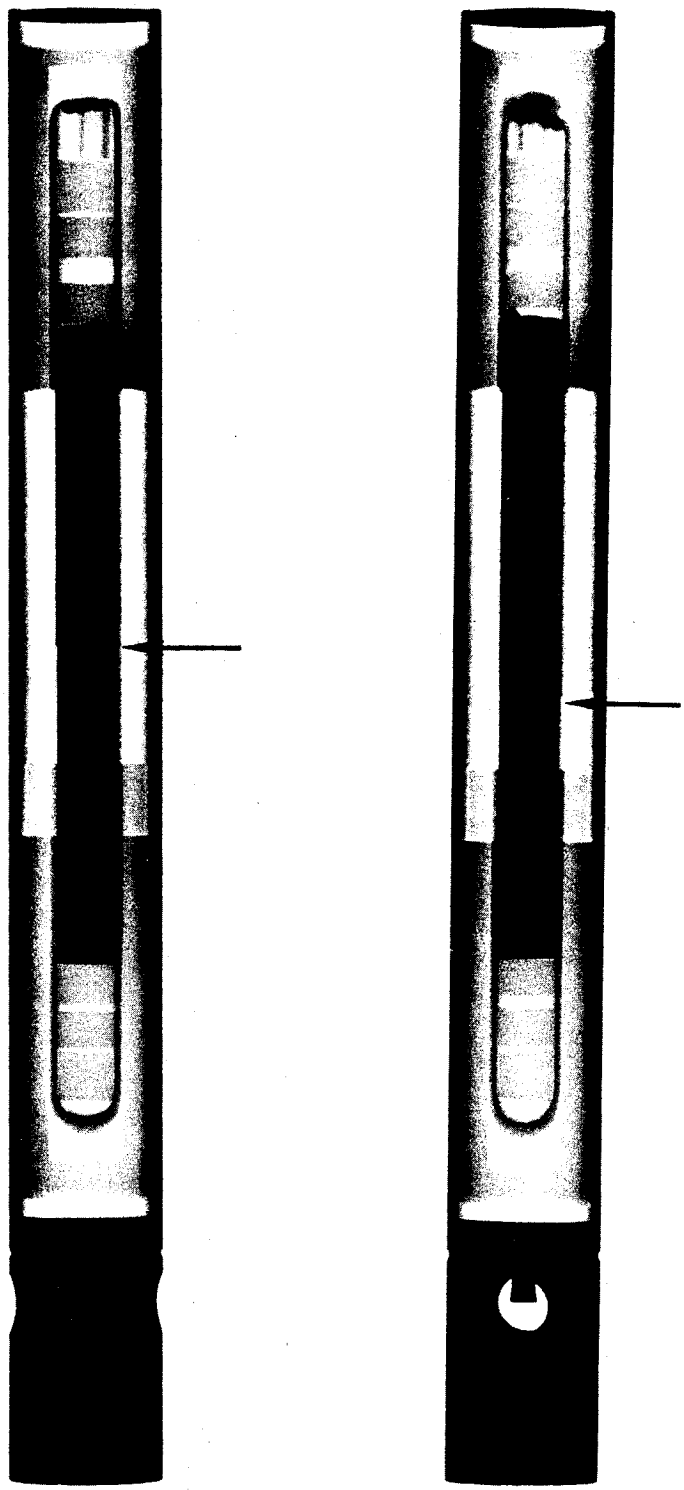

1A 3B

Figure 11. X-ray images of cartridges processed on the ground in a vertical position with the heater on top. Arrows indicate melt-back positions.

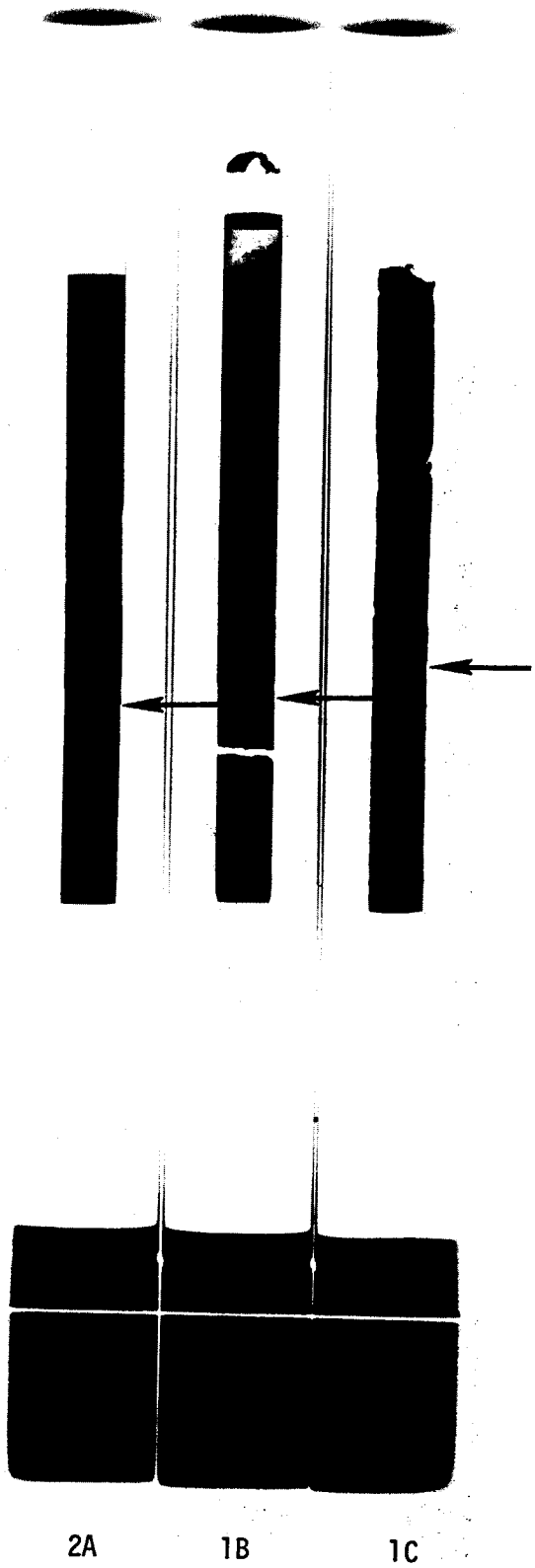

Figure 12. X-ray images of cartridges processed in SL-3. Arrows indicate melt-back positions.

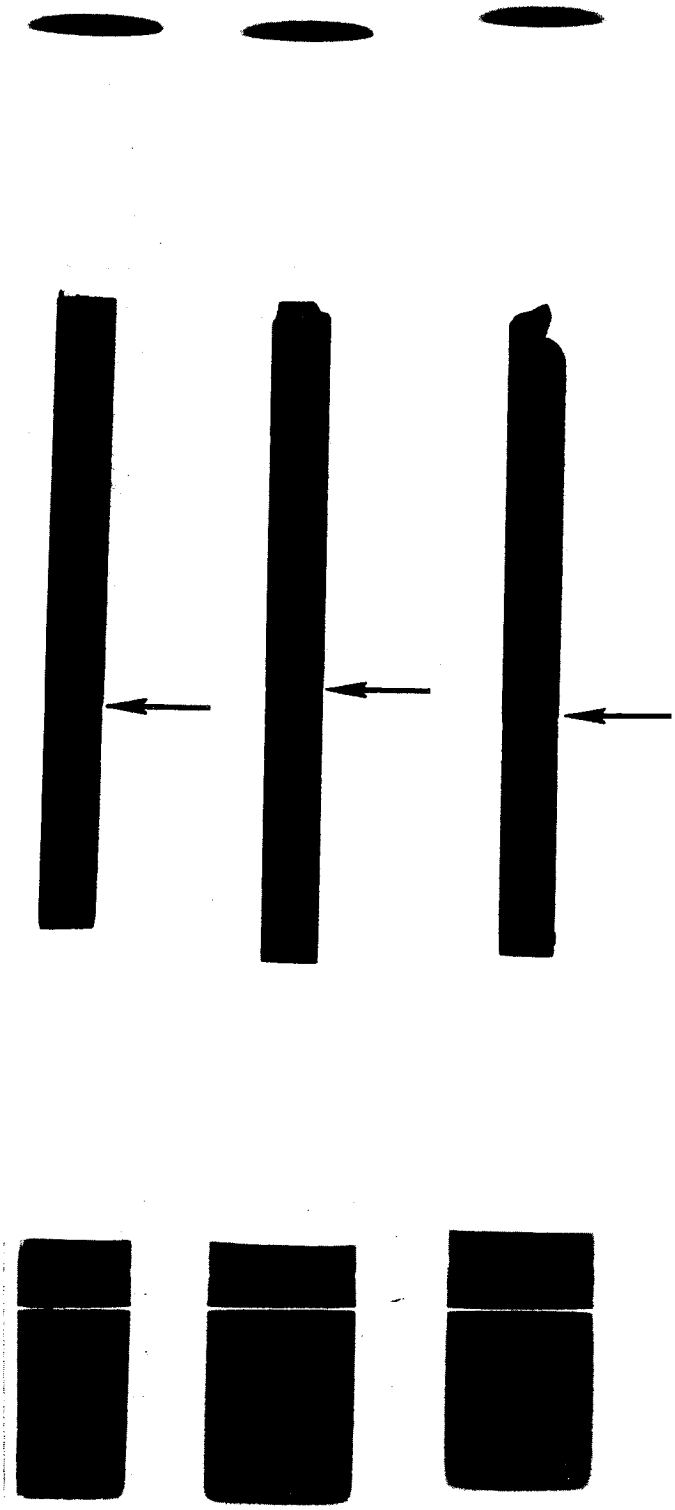

Figure 13. X-ray images of cartridges processed in SL-4. Arrows indicate melt-back positions.

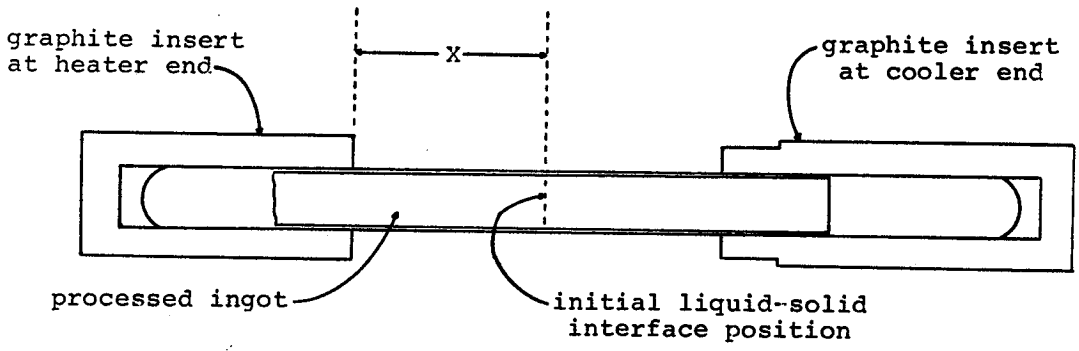

Figure 14. Definition of melt-back position

Free convection was clearly responsible--increasing the thermal transport in the melt without influencing that in the solid. Comparing ingot 3A to 4B, we see that the melting point and geometric effects cancelled. Comparing 4C to 3A, the melting point increase caused the melt-back to decrease, as expected. The first set of Skylab samples showed less meltback than the earth grown samples; from the geometric factors we would expect more meltback. This was probably due to the melt not contacting the ampoule wall. The second set of Skylab samples showed more melt-back due to the higher initial temperature of the heater.

The silica ampoules were removed from both the NASA and the USC processed ingots by soaking in HF for up to 2 days. The NASA samples were then sandblasted to reveal the external grain structure, as shown in Figure 15. In all ingots, the slowly refrozen region contained elongated grains. The original casting and the portion in the heater which refroze rapidly were both dendritic.

Both the NASA and the USC ingots were cut longitudinally with an abrasive wire saw. The horizontally-processed ingots were cut parallel to the gravitational field during solidification. One-half

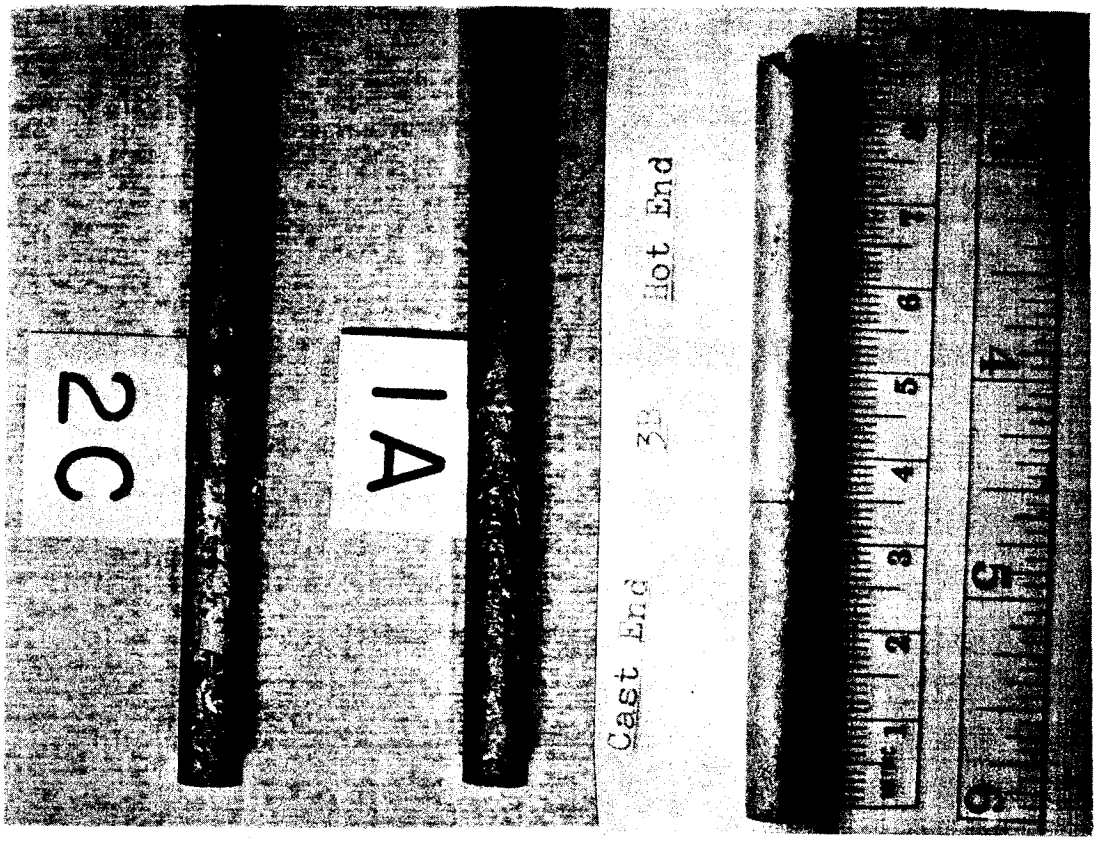

Figure 15(a). Sandblasted NASA ingots processed vertically. Furnace end on top.

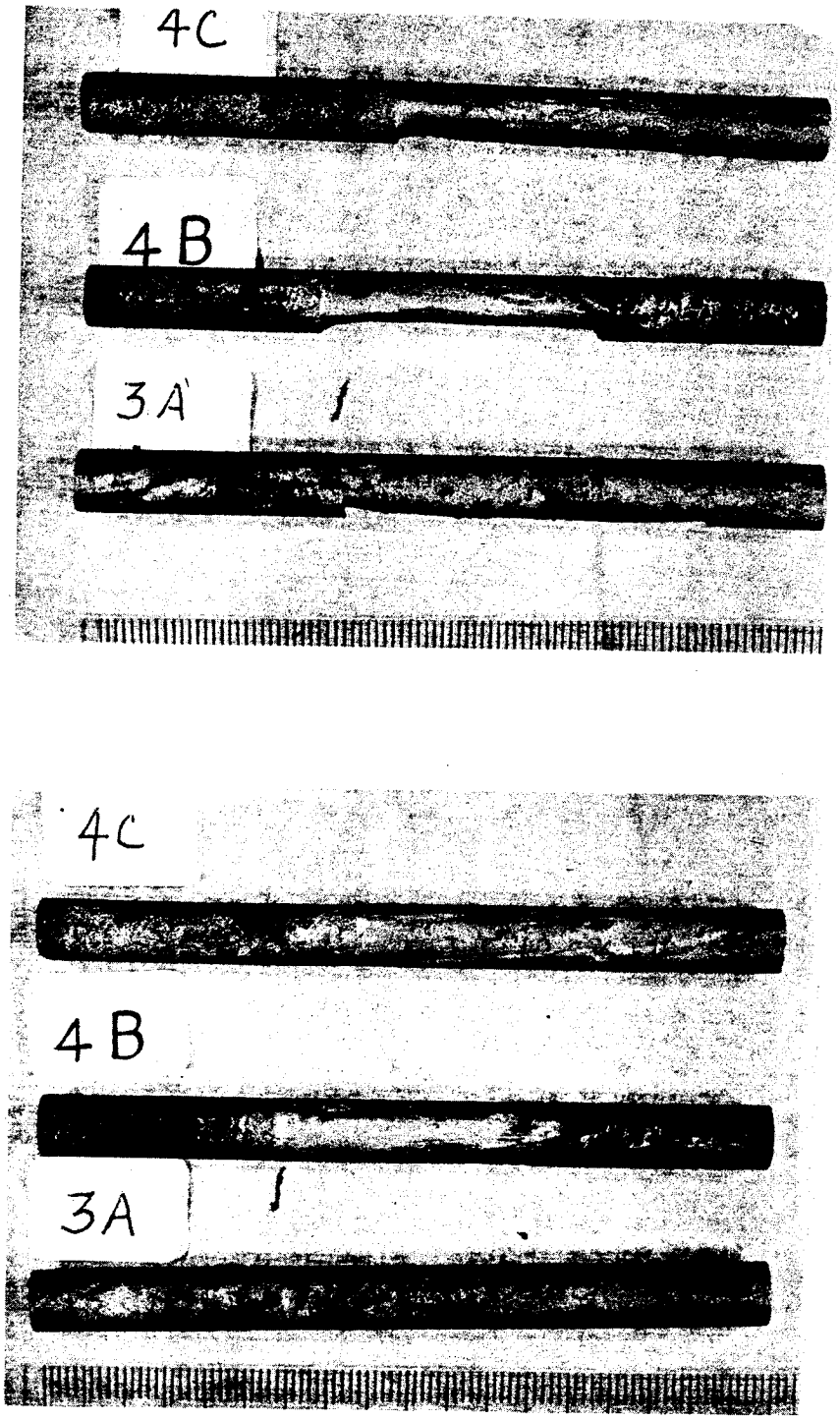

Figure 15(b). Sandblasted NASA ingots processed horizontally. Furnace end on right.

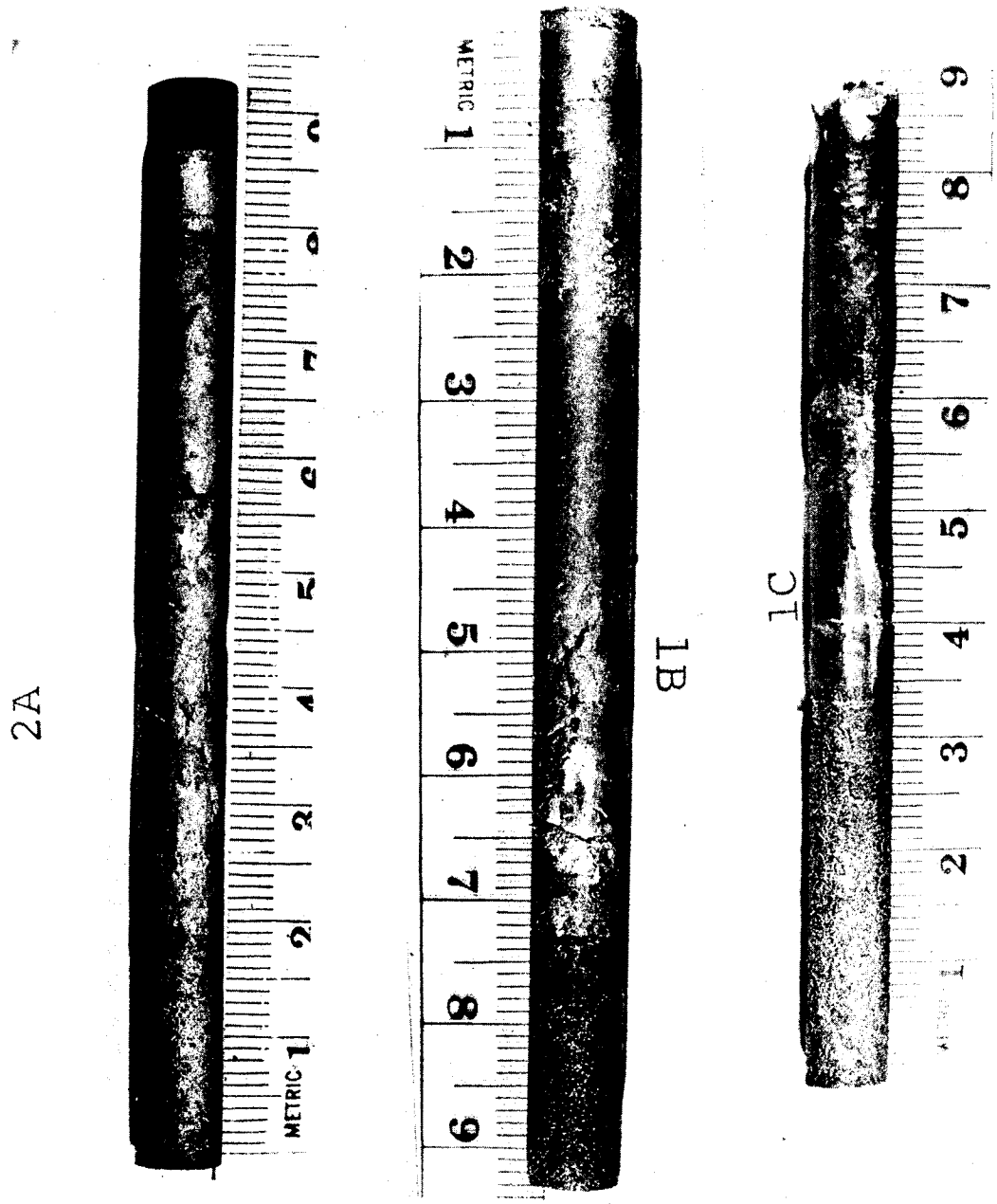

Figure 15(c). Sandblasted NASA ingots processed in SL-3. Furnace end on top.

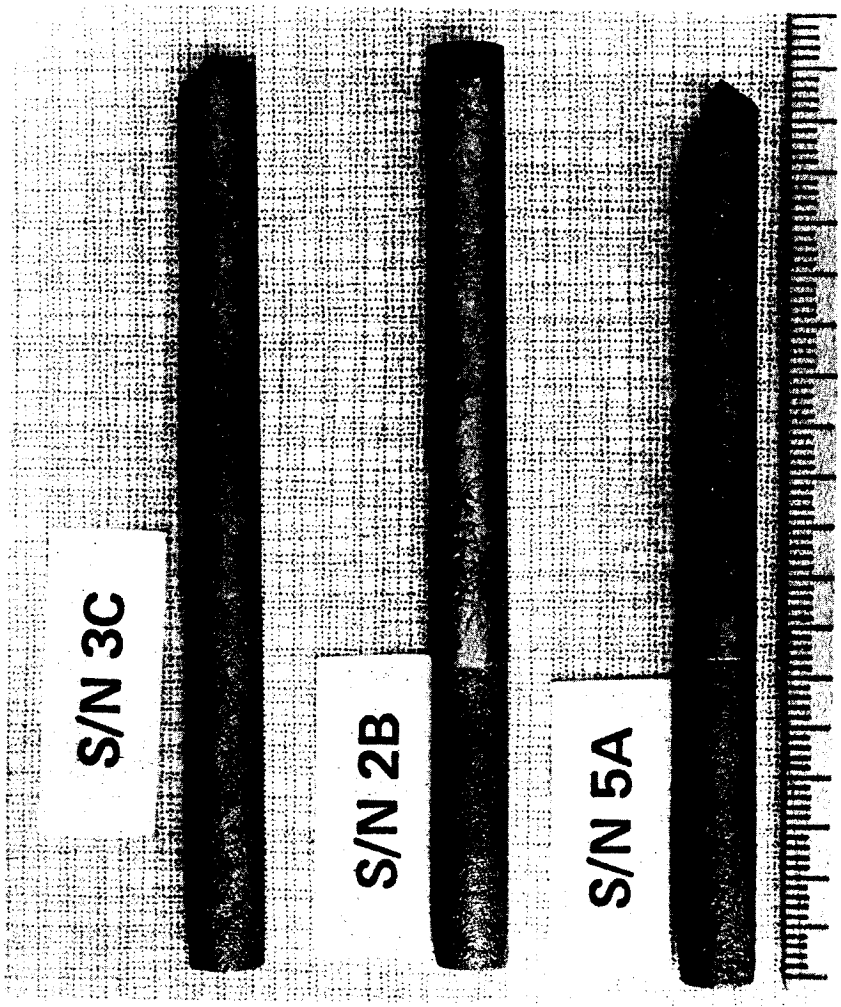

Figure 15(d). Sandblasted NASA ingots processed in SL-4. Furnace end on top.

1A

2C

Figure 15(e). Close up photographs of sandblasted NASA ingots processed vertically, with heater portion on top.

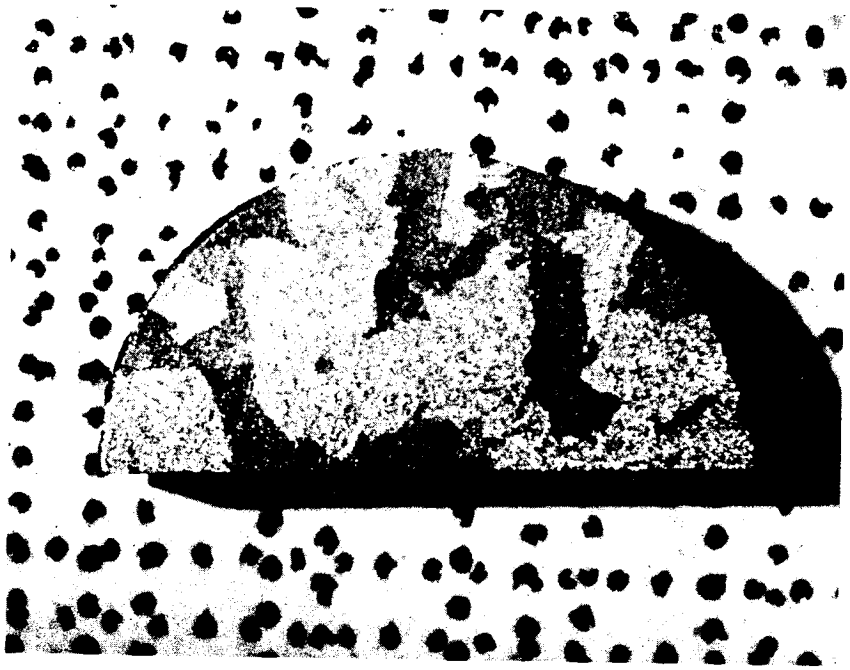

Figure 17(a). Sandblasted cross-sectional slice from ingot 1C (SL-3) about 4 mm from initial interface position.

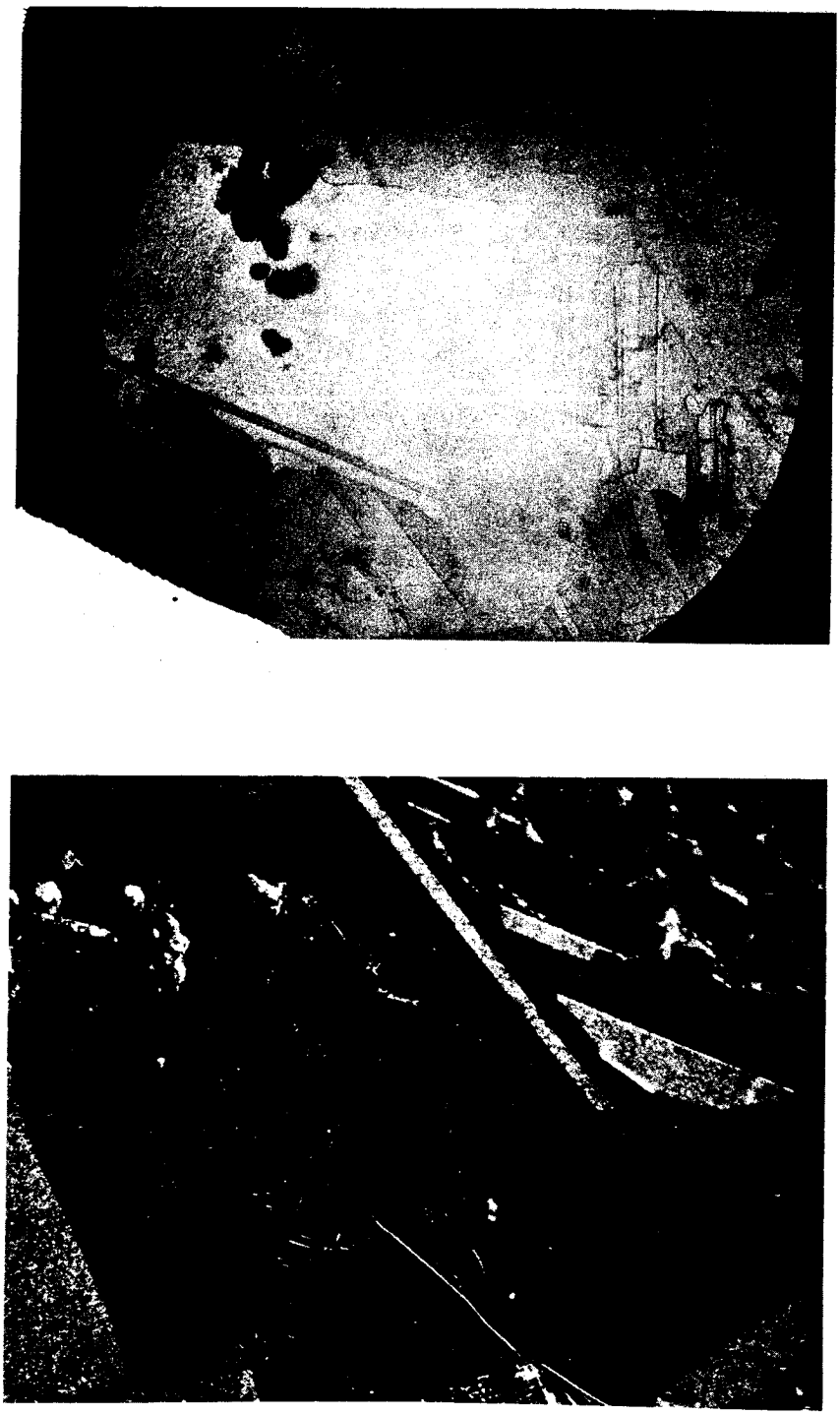

Figure 17(b). Cross-sectional slices of ingot 2C, processed vertically by NASA.

Etched in $2HF:2HA_c:3HNO_3$.

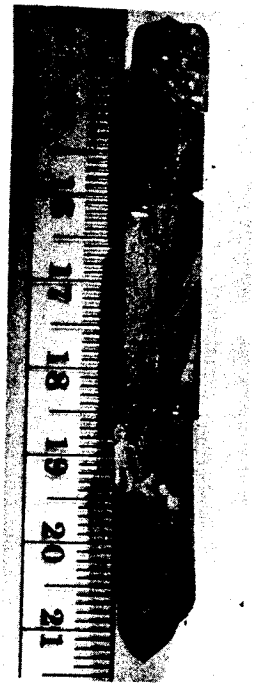

DF-9
$In_{0.5}Ga_{0.5}Sb$

DF-11
$In_{0.5}Ga_{0.5}Sb$

Figure 18(a). USC Bridgman-grown ingots.

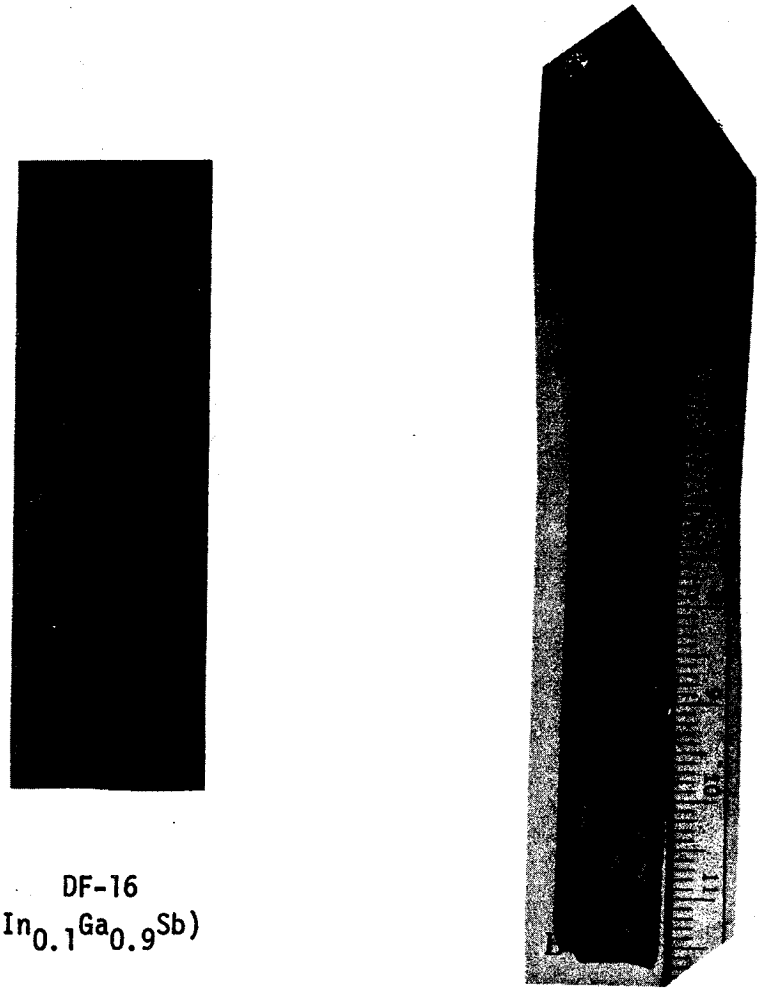

DF-16
($In_{0.1}Ga_{0.9}Sb$)

DF-17 ($In_{0.1}Ga_{0.9}Sb$)

Figure 18(b). USC Bridgman-Grown ingots.

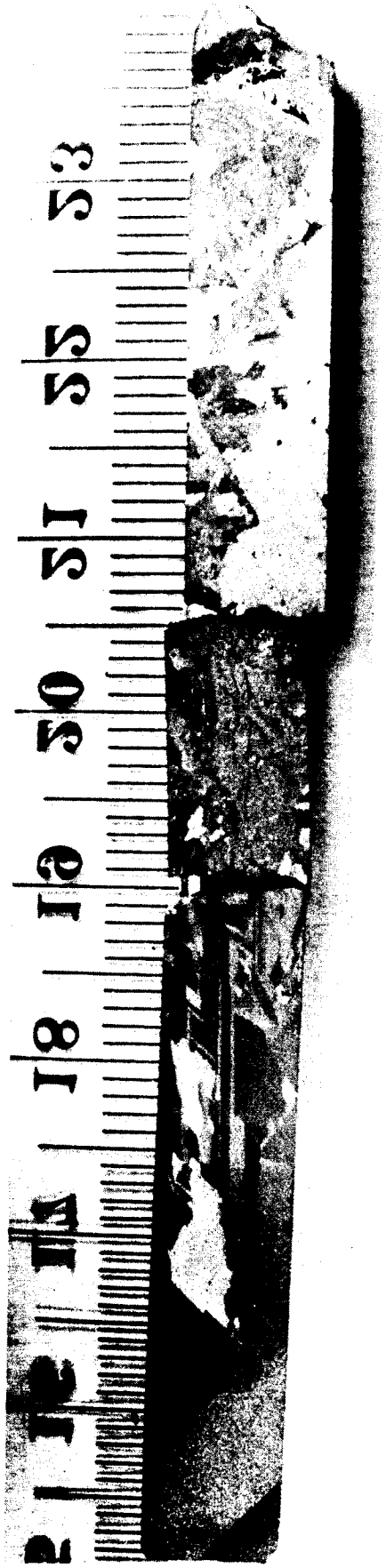

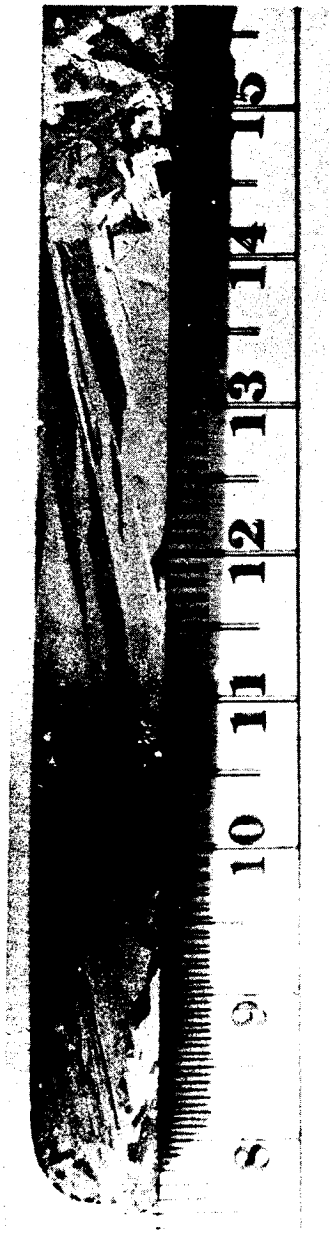

GF-6

GF-10

Figure 19. USC Gradient-frozen ingots of $In_{0.1}Ga_{0.9}Sb$.

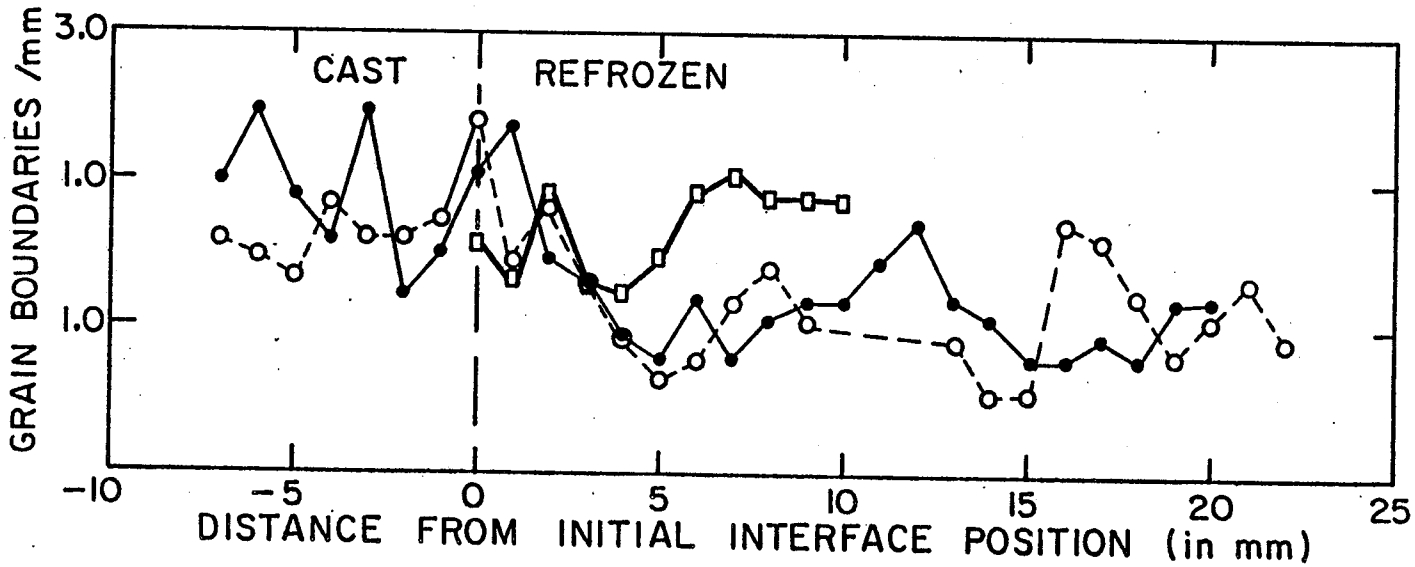

Figure 20. Distribution of grain boundaries in NASA $In_{0.5}Ga_{0.5}Sb$ ingots.

□ - Horizontally processed

○ - SL-3 processed

● - SL-4 processed

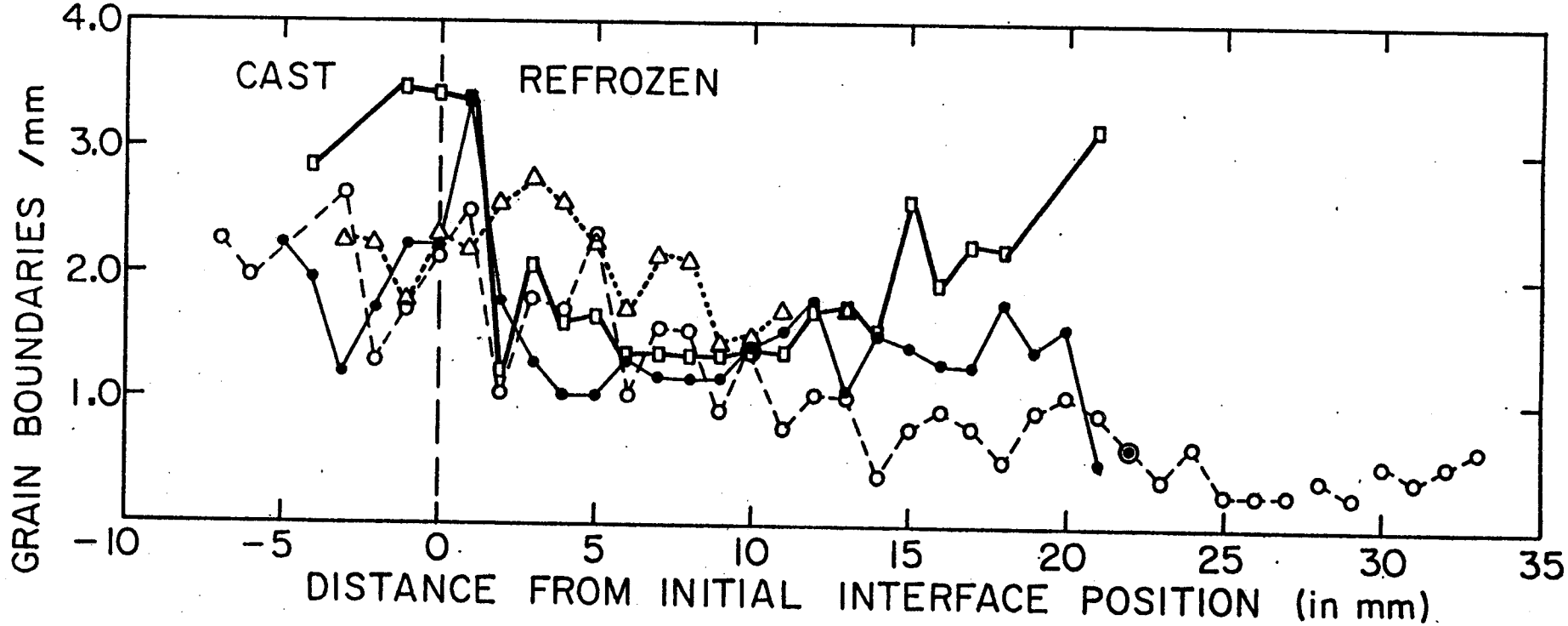

Figure 21. Distribution of grain boundaries in NASA $In_{0.3}Ga_{0.7}Sb$ ingots.

△ - Vertically processed

□ - Horizontally processed

○ - SL-3 processed

● - SL-4 processed

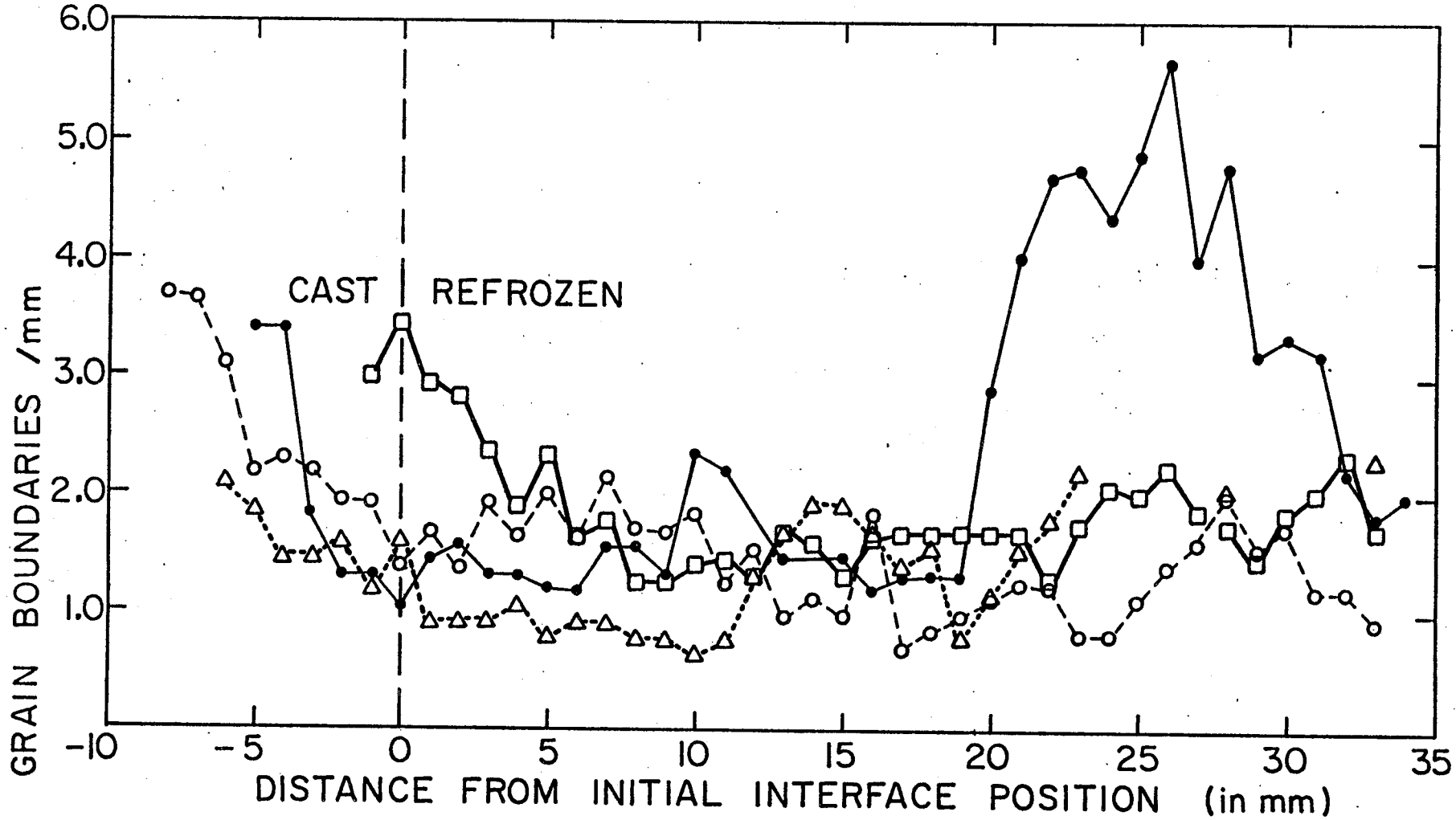

Figure 22. Distribution of grain boundaries in NASA $In_{0.1}Ga_{0.9}Sb$ ingots.

△ - Vertically processed

□ - Horizontally processed

○ - SL-3 processed

● - SL-4 processed

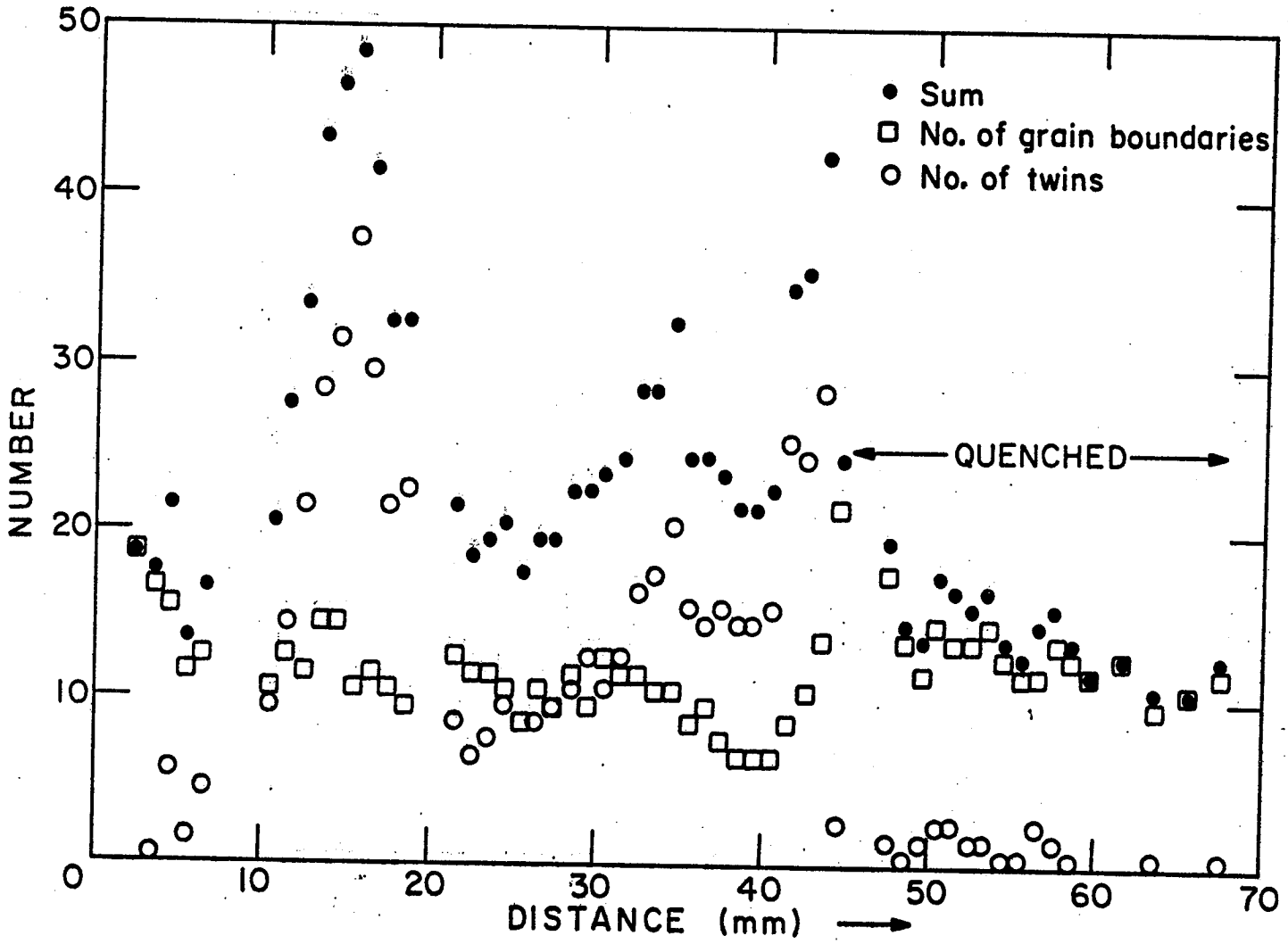

Figure 23(a). Distribution of grain and twin boundaries for USC Bridgman ingot DF-9 with original composition $In_{0.}$ $Ga_{0.}$ Sb.

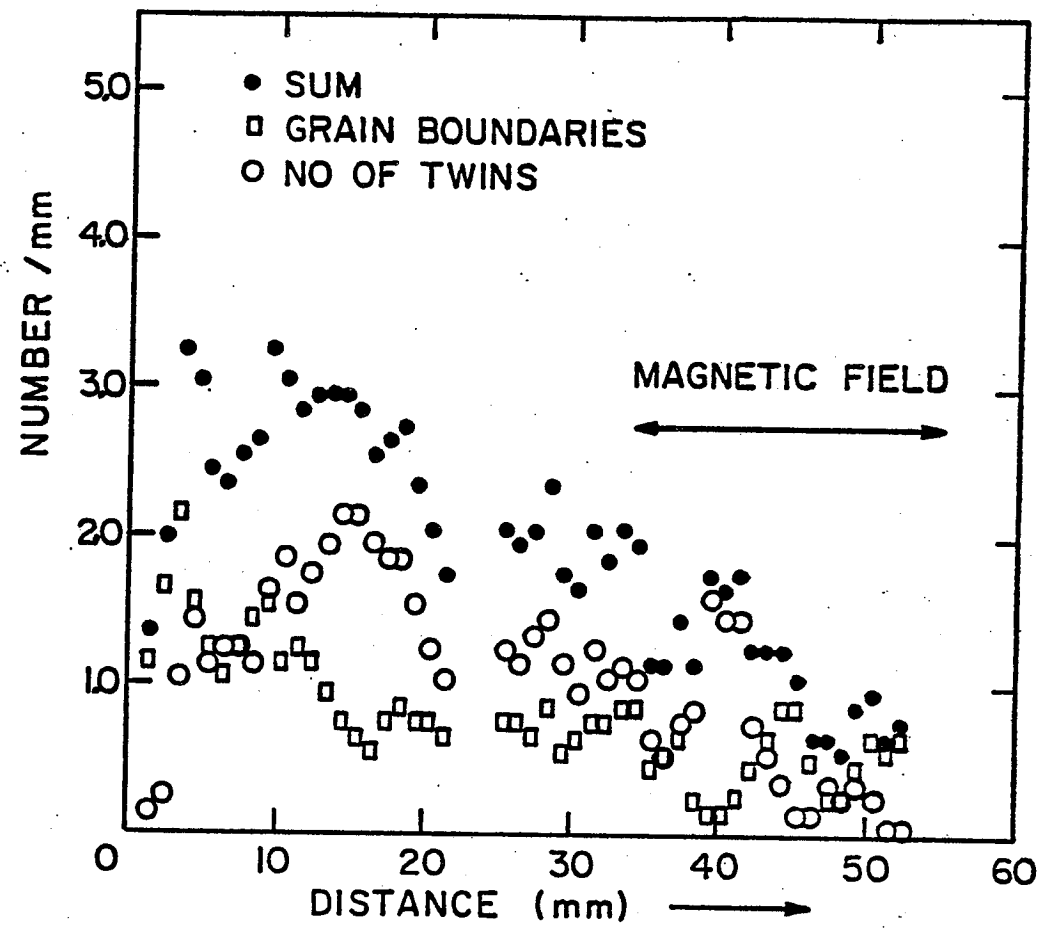

Figure 23(b). Distribution of grain and twin boundaries for USC Bridgman ingot DF-11 with original composition $In_{0.}$ $Ga_{0.}$ Sb.

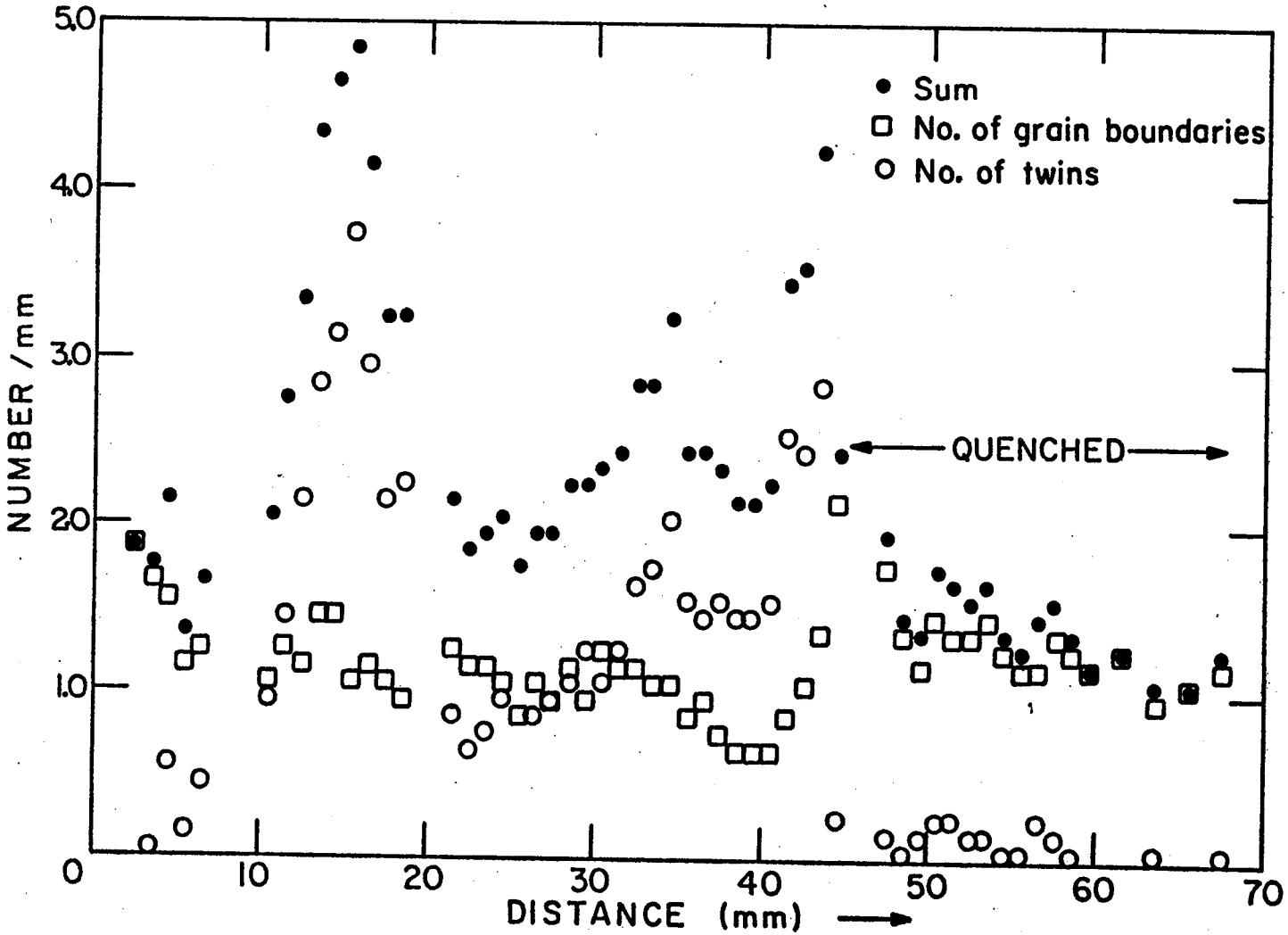

FIGURE 24. Distribution of grain boundaries and twin boundaries for sample DF-9 $In_{0.5}Ga_{0.5}Sb$

D. Twins

The number of twin boundaries was similarly counted, as shown in Figures 23-27. The number of twins increased at first, particularly in the earth-processed ingots. After the initial increase, the number of twins decreased, except in the horizontally-processed ingots. Twinning decreased as the In content of the initial melt increased. Twinning was much less in the space-processed ingots, particularly as the In concentration increased. The USC Bridgman experiments seem to indicate that imposition of the magnetic field caused twinning to decrease, but more experiments are needed to verify this.

E. Bubbles

Gas bubbles, or voids, were found in all of the NASA samples. Examples are shown in Figure 28. Since the NASA ampoules were back-filled with some helium, these were presumably filled with helium. The USC ampoules were sealed with a much lower gas pressure, and so no bubbles formed, as expected (5).

As shown in Figures 29-31, the void distribution was different in the earth-grown and space-grown samples. For the samples grown on earth, particularly those processed horizontally, the voids were concentrated at the initial liquid-solid interface. This congregation also served to show that the initial interface was planar, indicating that the heat flow was longitudinal as desired. For the samples grown horizontally, in addition to the voids at the initial interface, there were also voids along the side which was on top (at the free melt surface) during solidification. The space-processed ingots had voids dispersed throughout the slowly grown region. Those processed in SL-4 seemed to have somewhat fewer bubbles than the SL-3 ingots.

F. Cracks

Figures 15 and 16 show that microcracks developed in the ingots. Examination of the grain structure near the cracks indicated that some cracks inhibited grain growth, others initiated new grains,

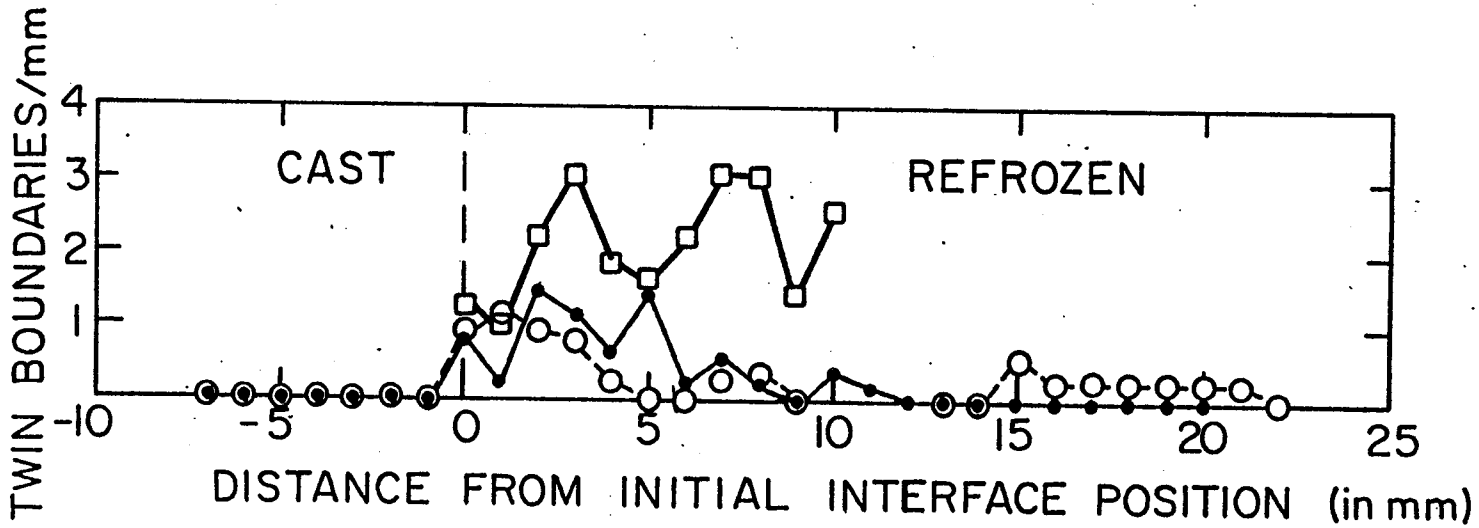

Figure 25. Distribution of twin boundaries in NASA $In_{0.5}Ga_{0.5}Sb$ ingots.

□ - Horizontally processed

○ - SL-3 processed

● - SL-4 processed

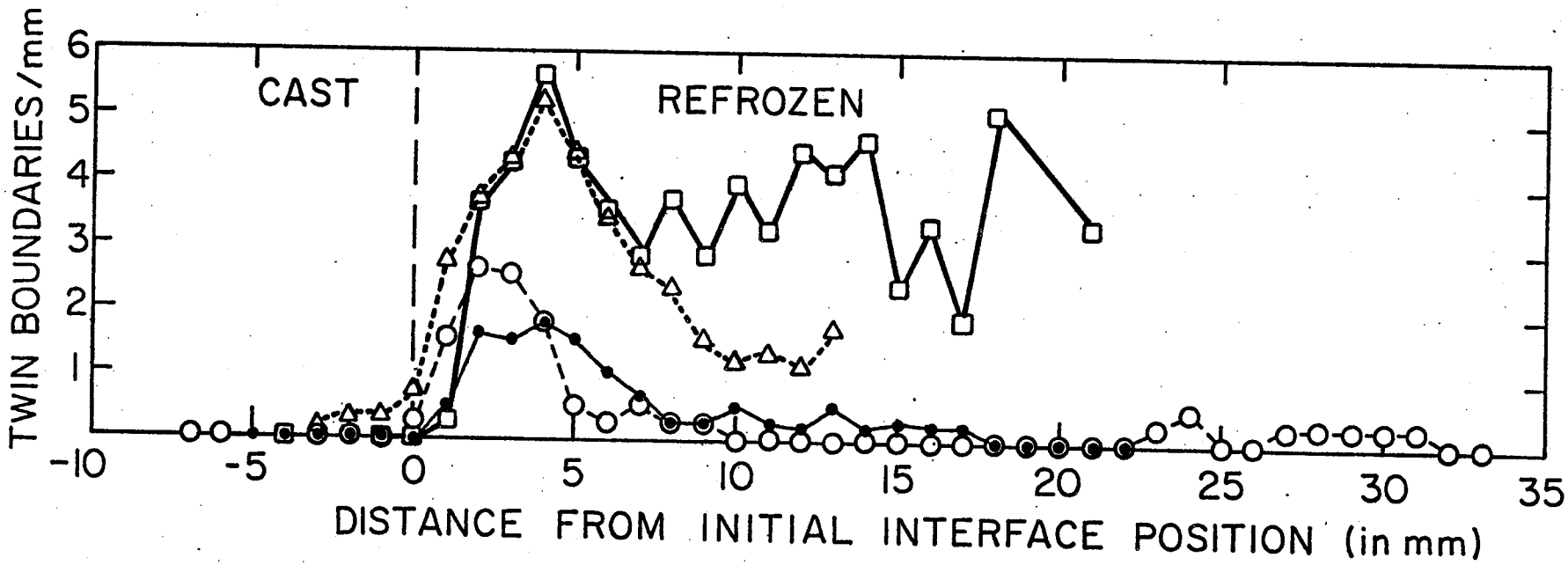

Figure 26. Distribution of twin boundaries in NASA $In_{0.3}Ga_{0.7}Sb$ ingots.

□ - Vertically processed

△ - Horizontally processed

○ - SL-3 processed

● - SL-4 processed

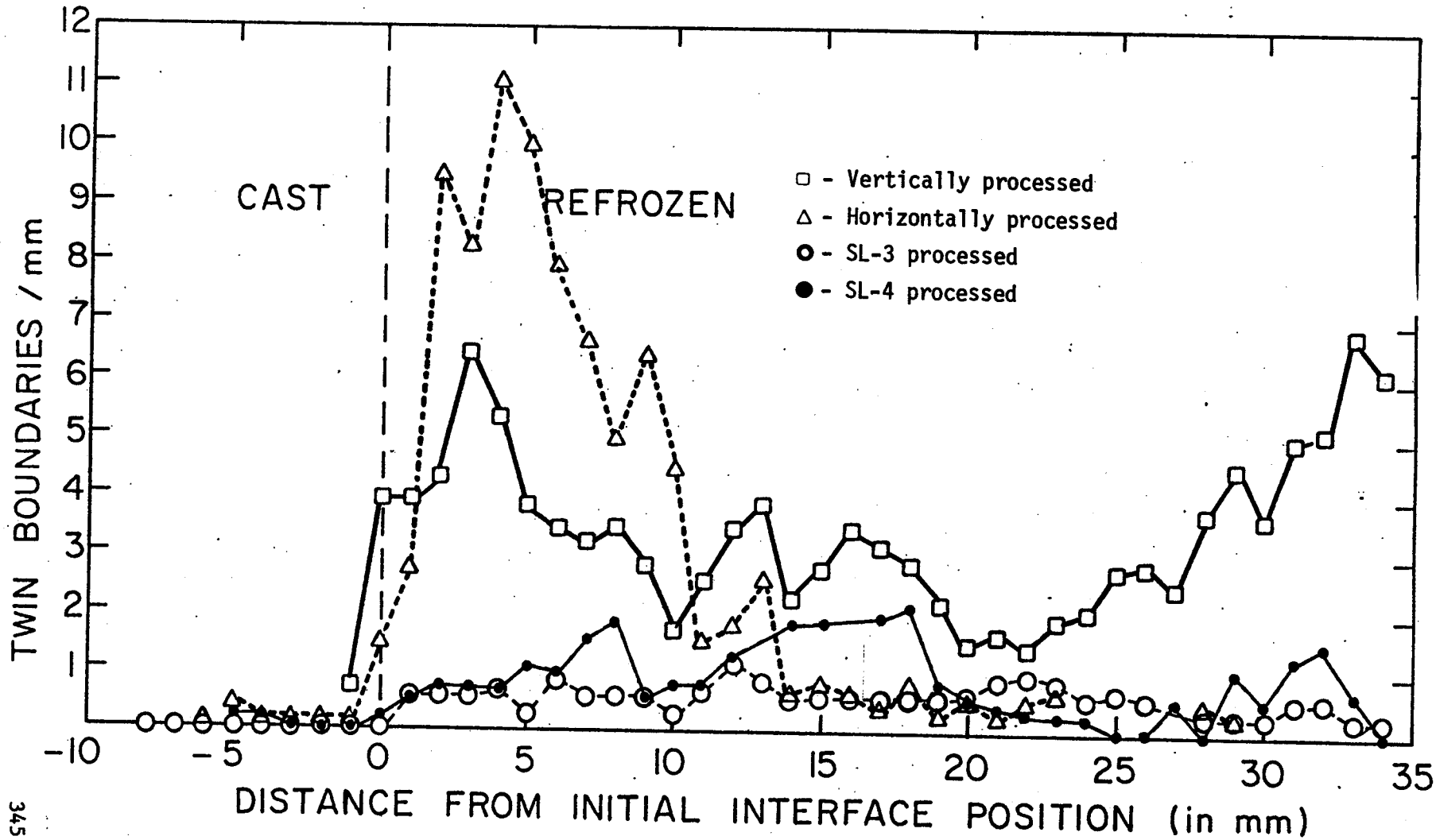

FIGURE 27. DISTRIBUTION OF TWIN BOUNDARIES IN NASA $In_{0.1}Ga_{0.9}Sb$.

3A

4A

Figure 28(a). Gas bubbles as seen on cross-sectional slices of NASA horizontally processed ingots, near initial interface.

Figure 28(b). Gas bubbles as seen in SL-3 ingot 1B.

Figure 28(c). Gas bubbles as seen in SL-3 ingot 2A.

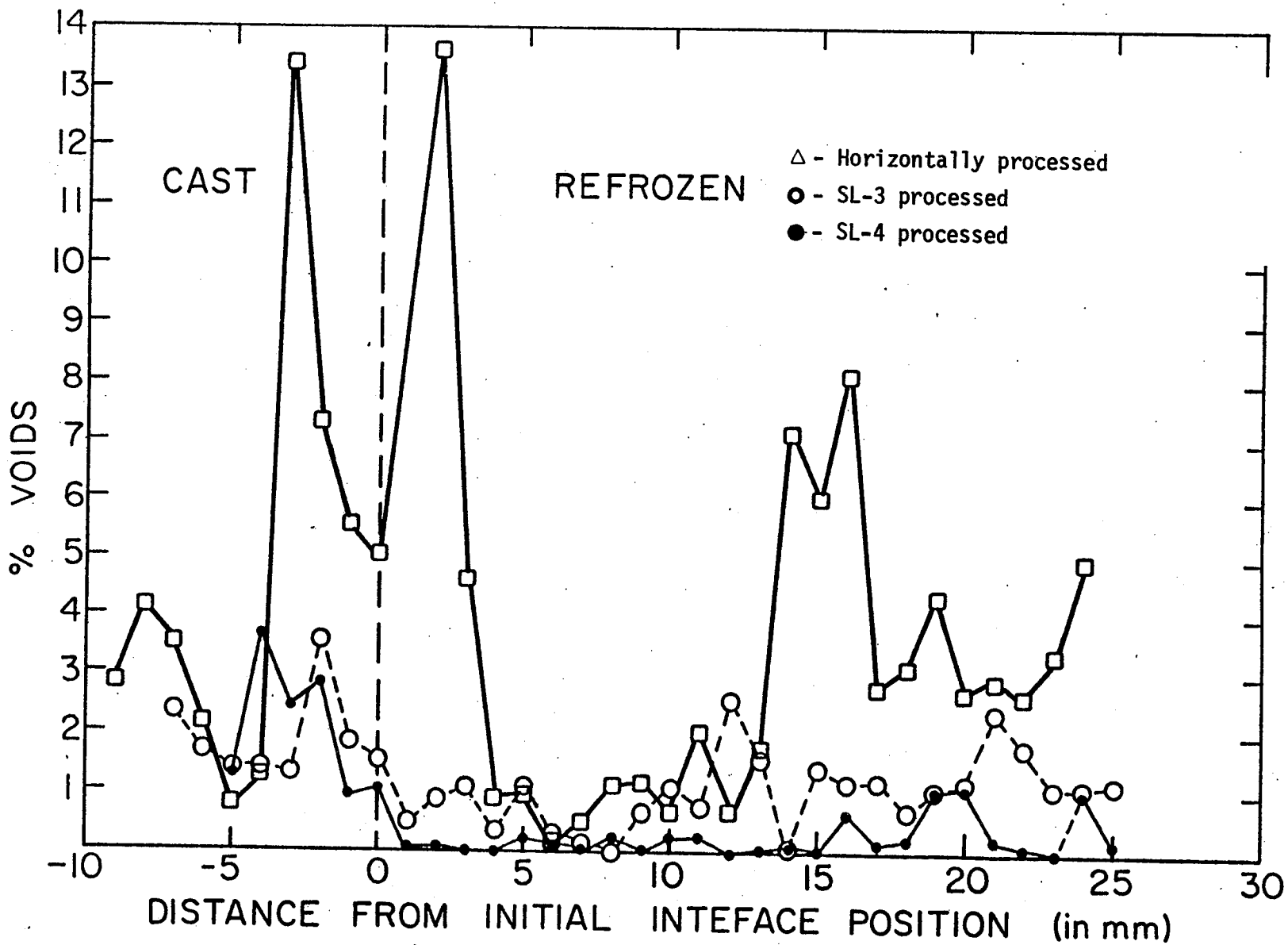

FIGURE 29. VOID DISTRIBUTION IN NASA $In_{0.5}Ga_{0.5}Sb$ INGOTS

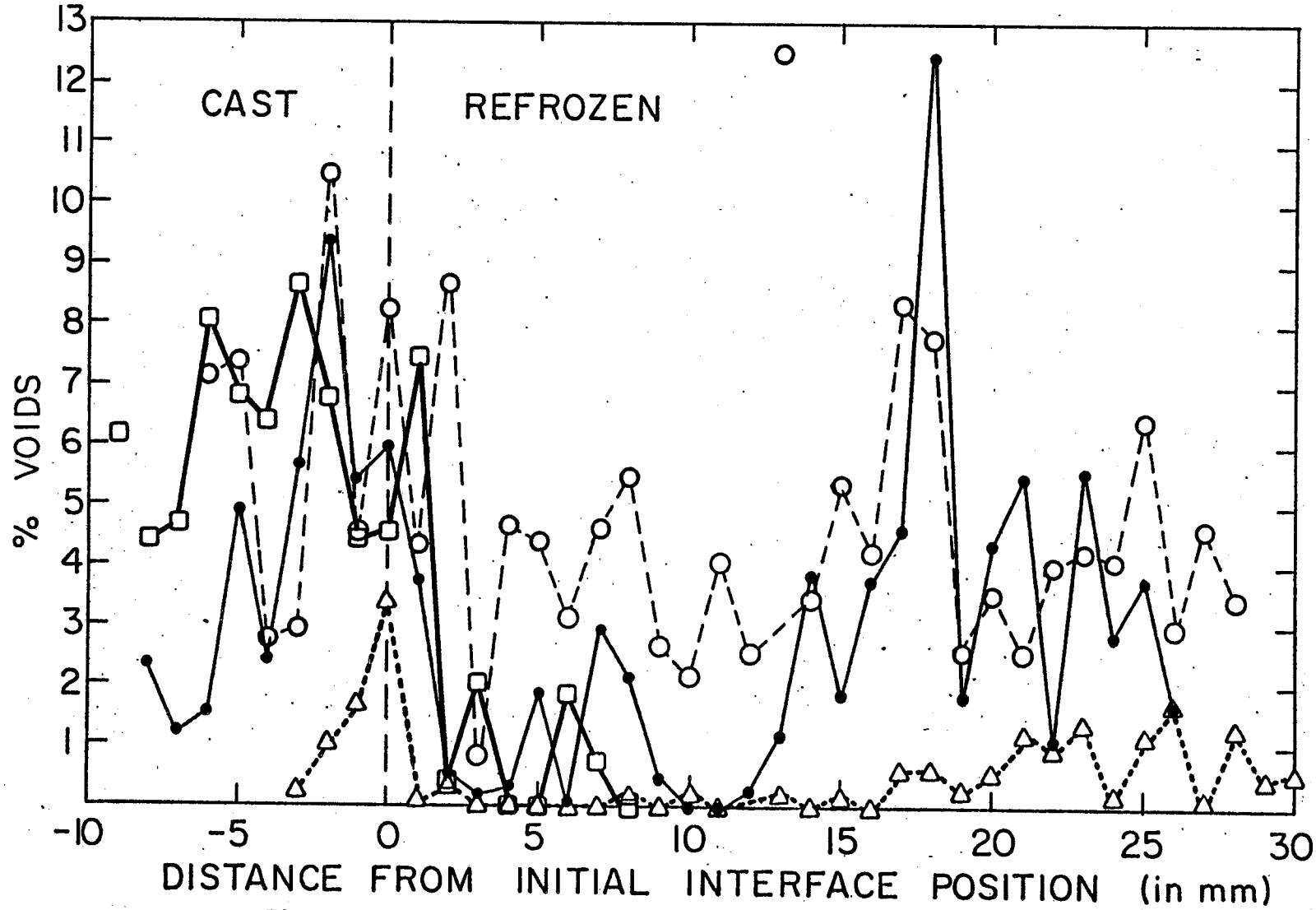

Figure 30. Void distribution in NASA $In_{0.3}Ga_{0.7}Sb$ ingots.

□ - Vertically processed

△ - Horizontally processed

○ - SL-3 processed

● - SL-4 processed

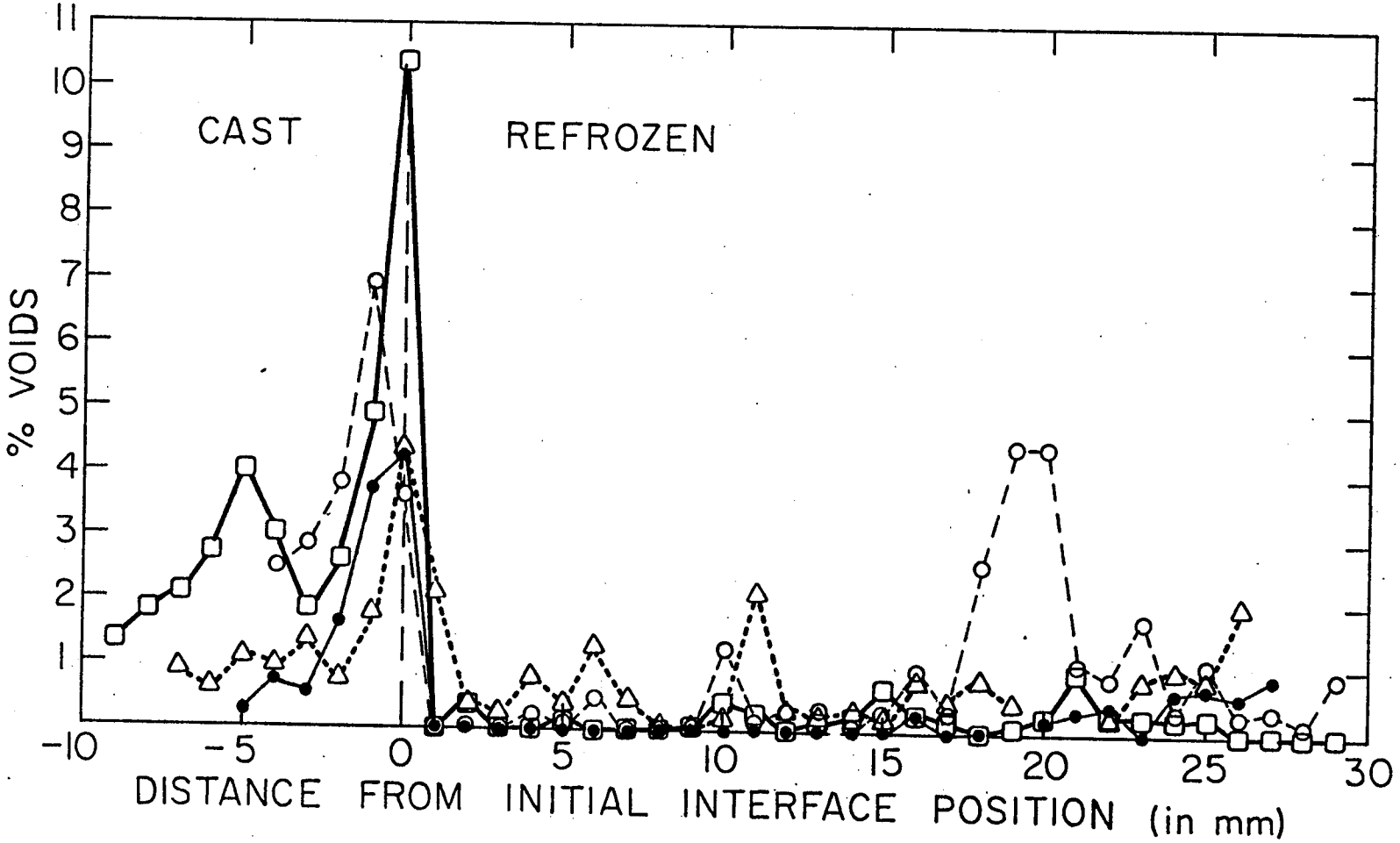

Figure 31. Void distribution in NASA $In_{0.1}Ga_{0.9}Sb$ ingots.

□ - Vertically processed

△ - Horizontally processed

O - SL-3 processed

● - SL-4 processed

and still others did not appear to influence the grain structure. The latter probably developed after solidification during the cool-down. At some cracks, the growth direction of the grains changed.

The distribution of cracks was counted by the same method used for grain boundaries and twins. As shown in Figures 32-34 there were more cracks in the cast portions and the last regrown regions. This is probably due to compositional stresses brought about by constitutional-supercooling generated inhomogeneities.

G. Atomic Absorption Analyses

A Perkin Elmer 306 Atomic Absorption Spectrophotometer was used to analyze for average Ga and In concentration of every third or fourth cross-sectional slice of all NASA ingots. Each slice was ultrasonically cleaned in acetone, chemically polished with 2 HF:3 HNO_3:2 HAc, rinsed in methanol, dried, weighed, dissolved in 5% HCℓ, diluted with deionized water, and analyzed. Figures 35-37 show that the vertically-processed and the Skylab-processed ingots had nearly identical concentration profiles. The concentration profiles in the horizontally-processed ingots are quite different because of the free convective stirring present in those runs. Note also the changes in concentration in the cast portions. These must have occurred during the soak period prior to programming down the heater. Since the castings were not homogeneous, the solid-liquid interface would actually have been a two-phase "mushy zone" in which recrystallization and compositional redistribution would be fairly rapid.

H. Electron Microprobe Analyses

The longitudinal slices were cut into one-inch lengths and final polished. These were analyzed at one millimeter intervals with an electron microprobe in the In characteristic X-ray mode. At least three passes were made over the length of the sample. The results are shown in Figure 38. The scatter which began to occur after several mm of resolidification is indicative of a non-planar interface caused by

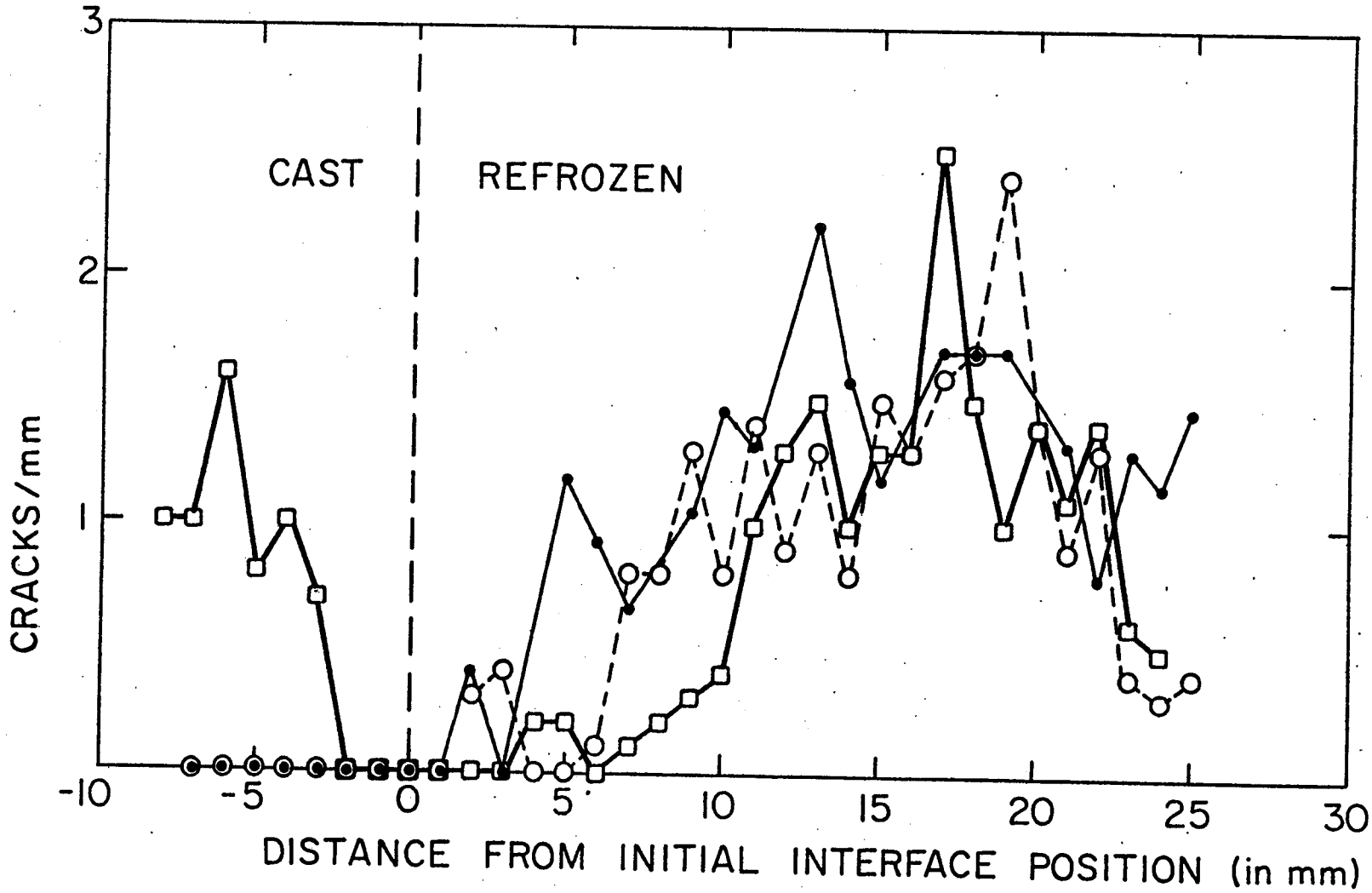

Figure 32. Crack distribution in NASA $In_{0.5}Ga_{0.5}Sb$ ingots.

□- Horizontally processed

O- SL-3 processed

●- SL-4 processed

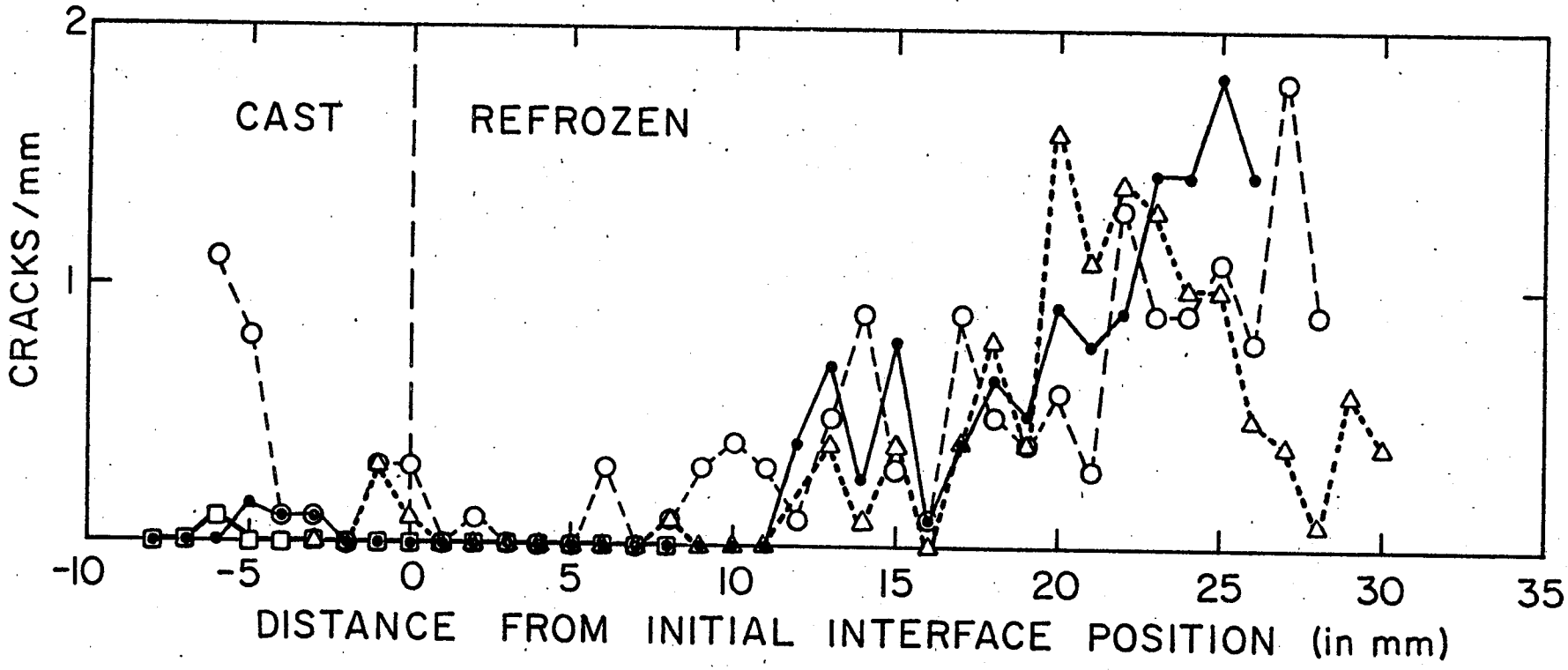

Figure 33. Crack distribution in NASA $In_{0.3}Ga_{0.7}Sb$ ingots.

△ - Vertically processed

□ - Horizontally processed

○ - SL-3 processed

● - SL-4 processed

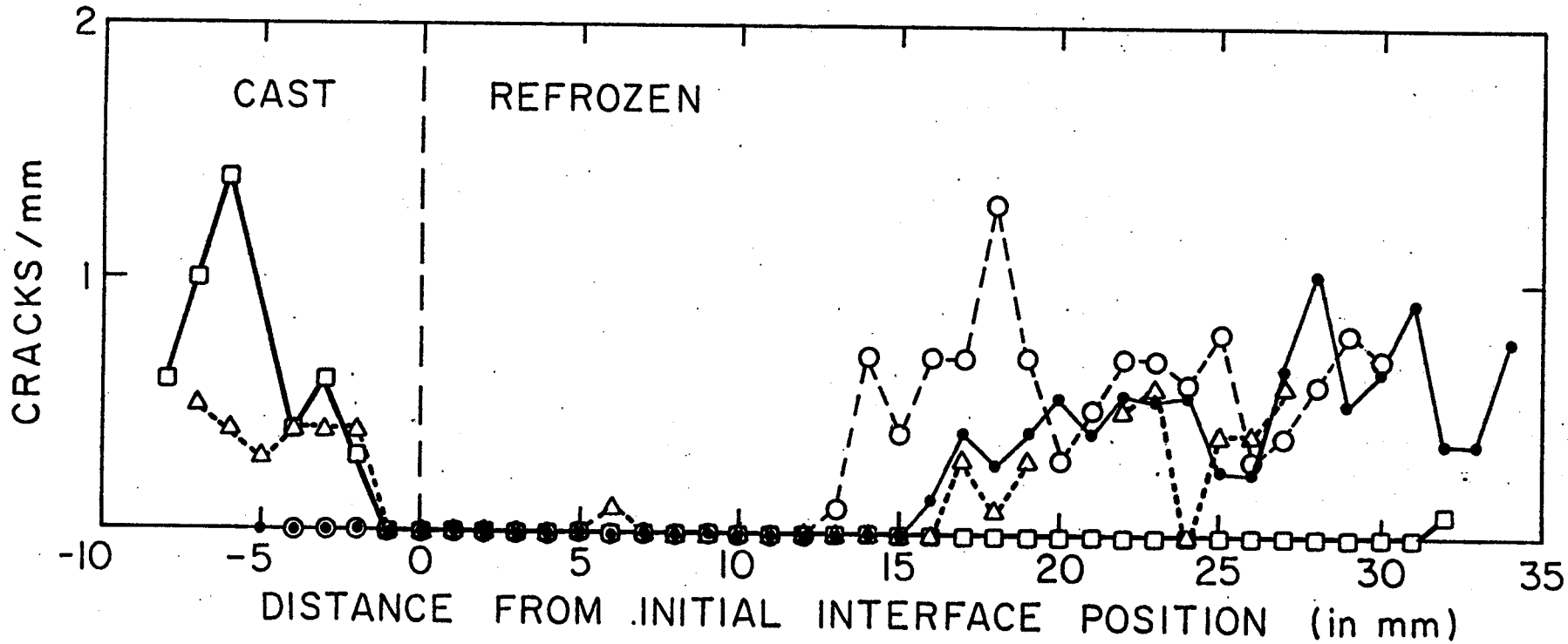

Figure 34. Crack distribution in NASA $In_{0.1}Ga_{0.9}Sb$ ingots.

△- Vertically processed

□- Horizontally processed

O- SL-3 processed

●- SL-4 processed

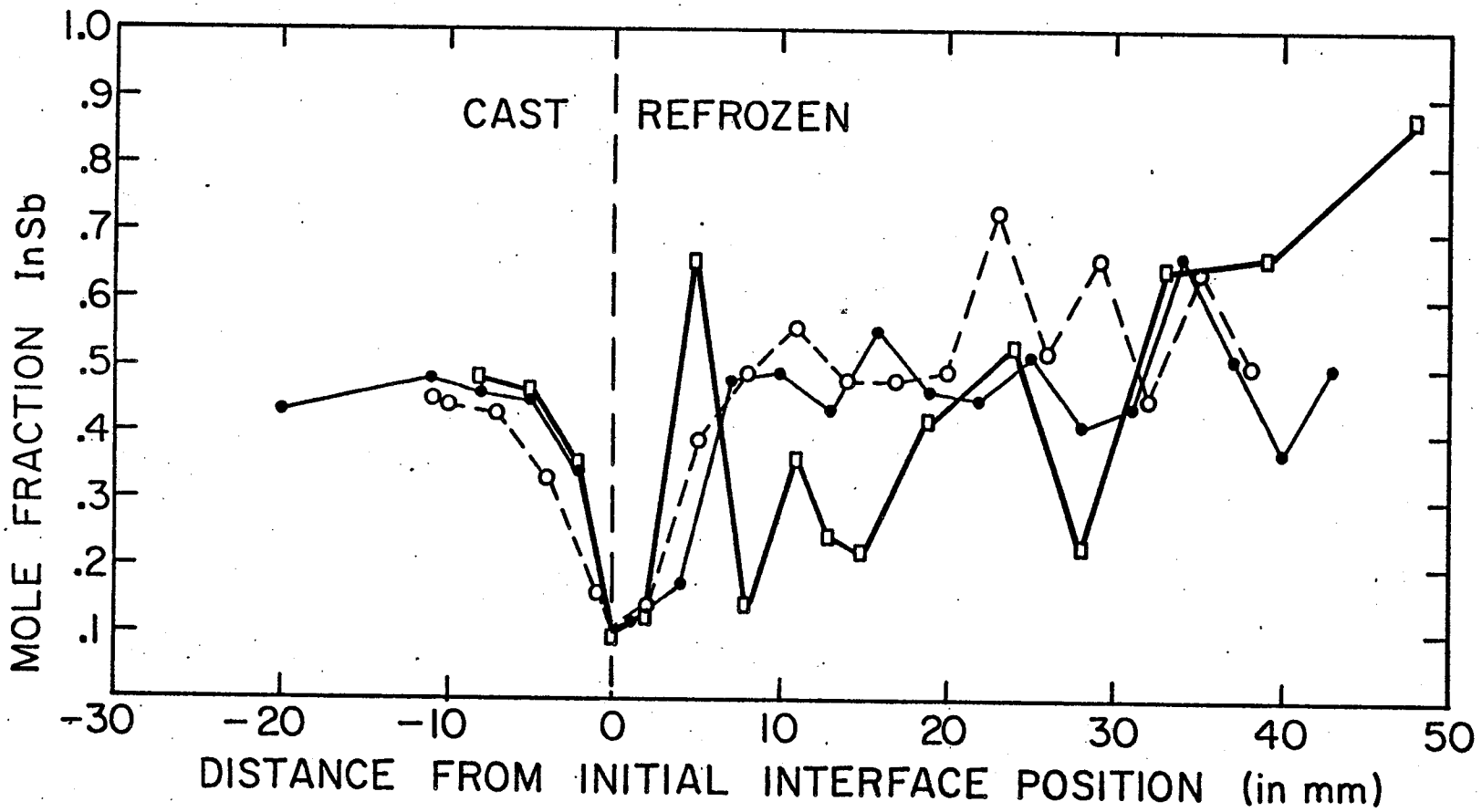

Figure 35. Indium concentration profiles in NASA $In_{0.5}Ga_{0.5}Sb$ ingots, as determined by atomic absorption spectrometry.

□ - Horizontally processed

○ - SL-3 processed

● - SL-4 processed

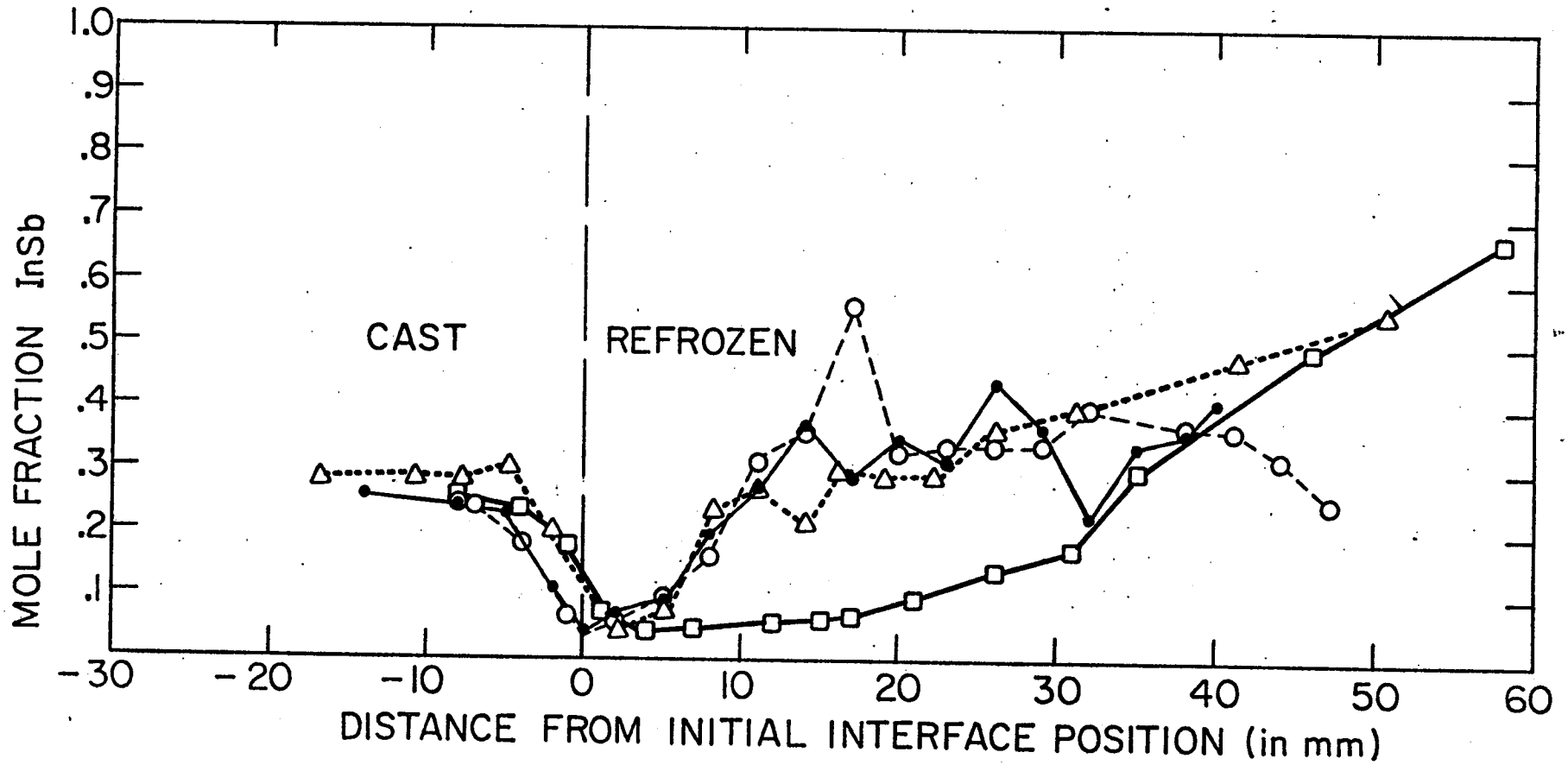

Figure 36. Indium concentration profiles in NASA $In_{0.3}Ga_{0.7}Sb$ ingots, as determined by atomic absorption spectrometry.

△ - Vertically processed

□ - Horizontally processed

○ - SL-3 processed

● - SL-4 processed

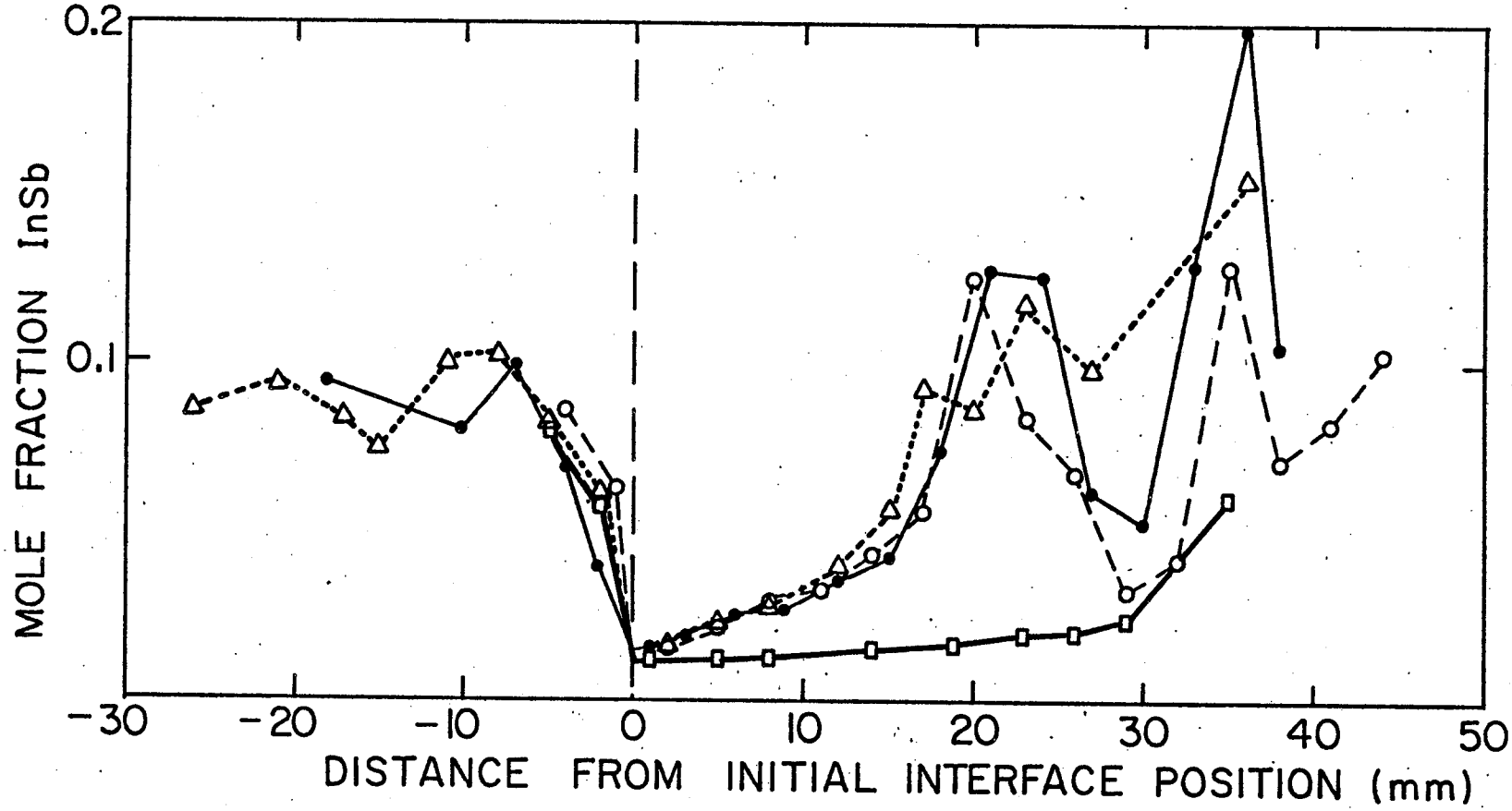

Figure 37. Indium concentration profiles in NASA $In_{0.1}Ga_{0.9}Sb$ ingots, as determined by atomic absorption spectrometry.

△ - Vertically processed

□ - Horizontally processed

○ - SL-3 processed

● - SL-4 processed

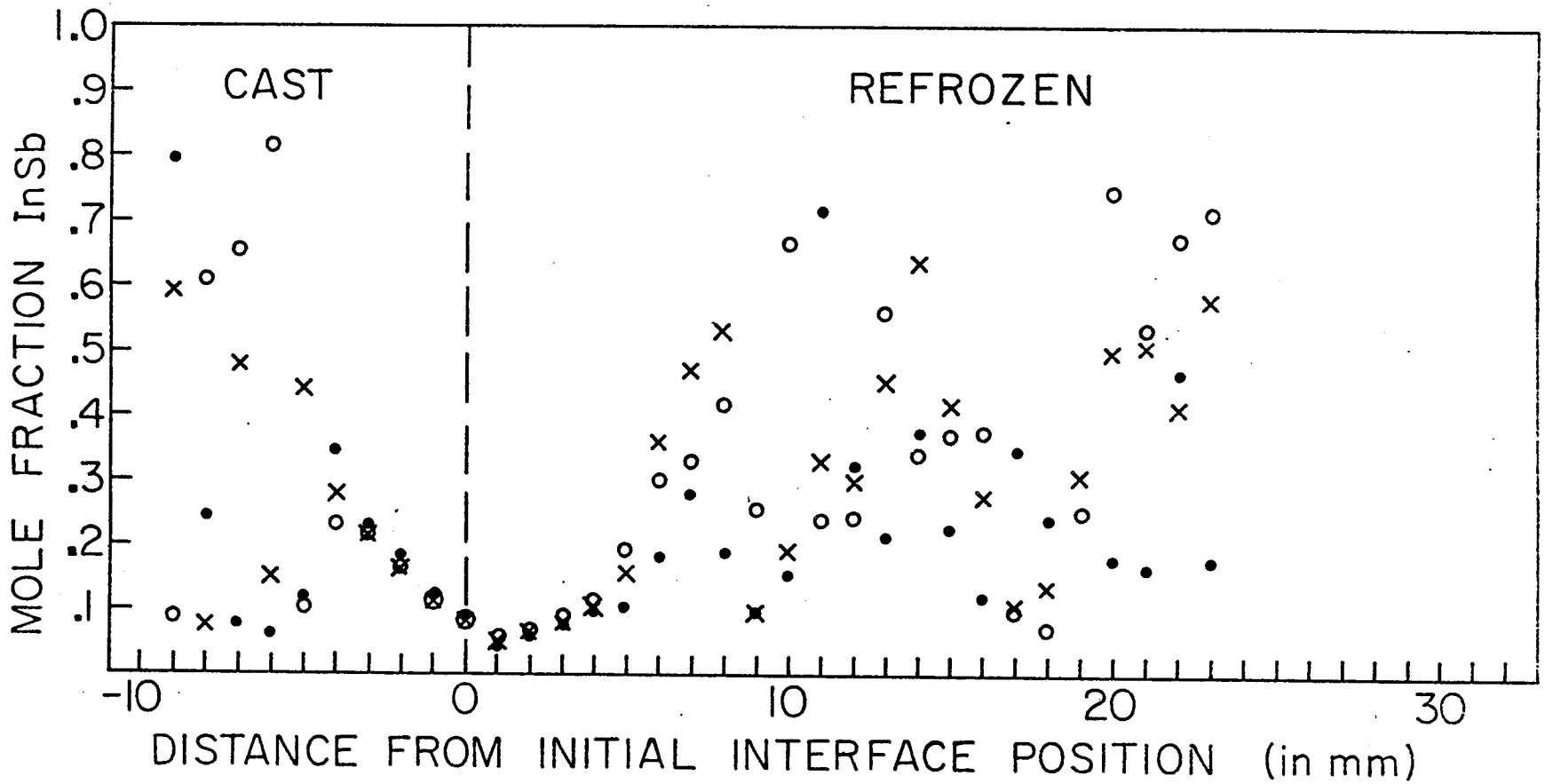

Figure 38. Electron microprobe results on NASA ingot 3B ($In_{0.3}Ga_{0.7}Sb$ processed vertically).

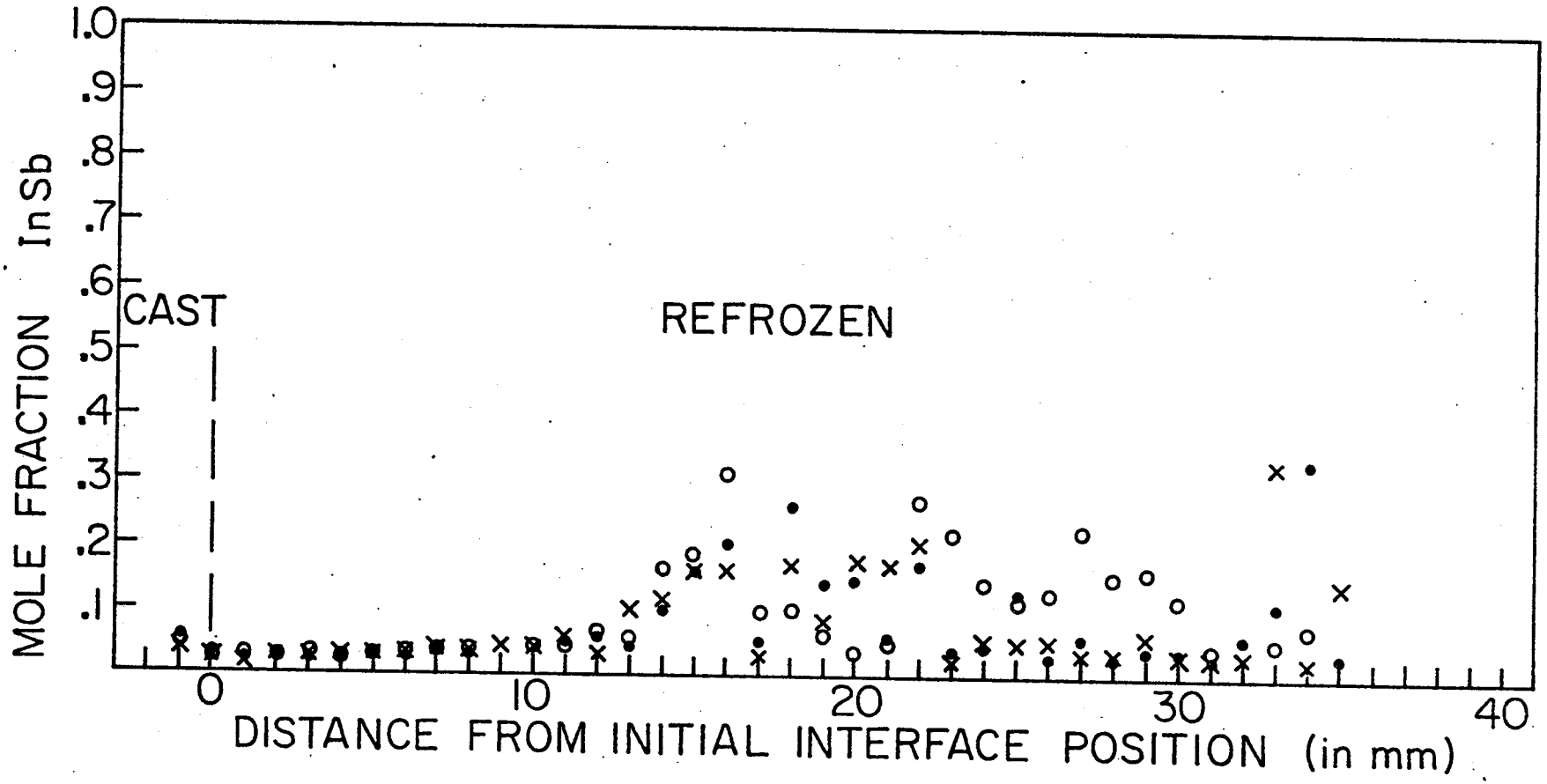

Figure 39. Electron microprobe results on NASA ingot 2C ($In_{0.1}Ga_{0.9}Sb$ processed vertically).

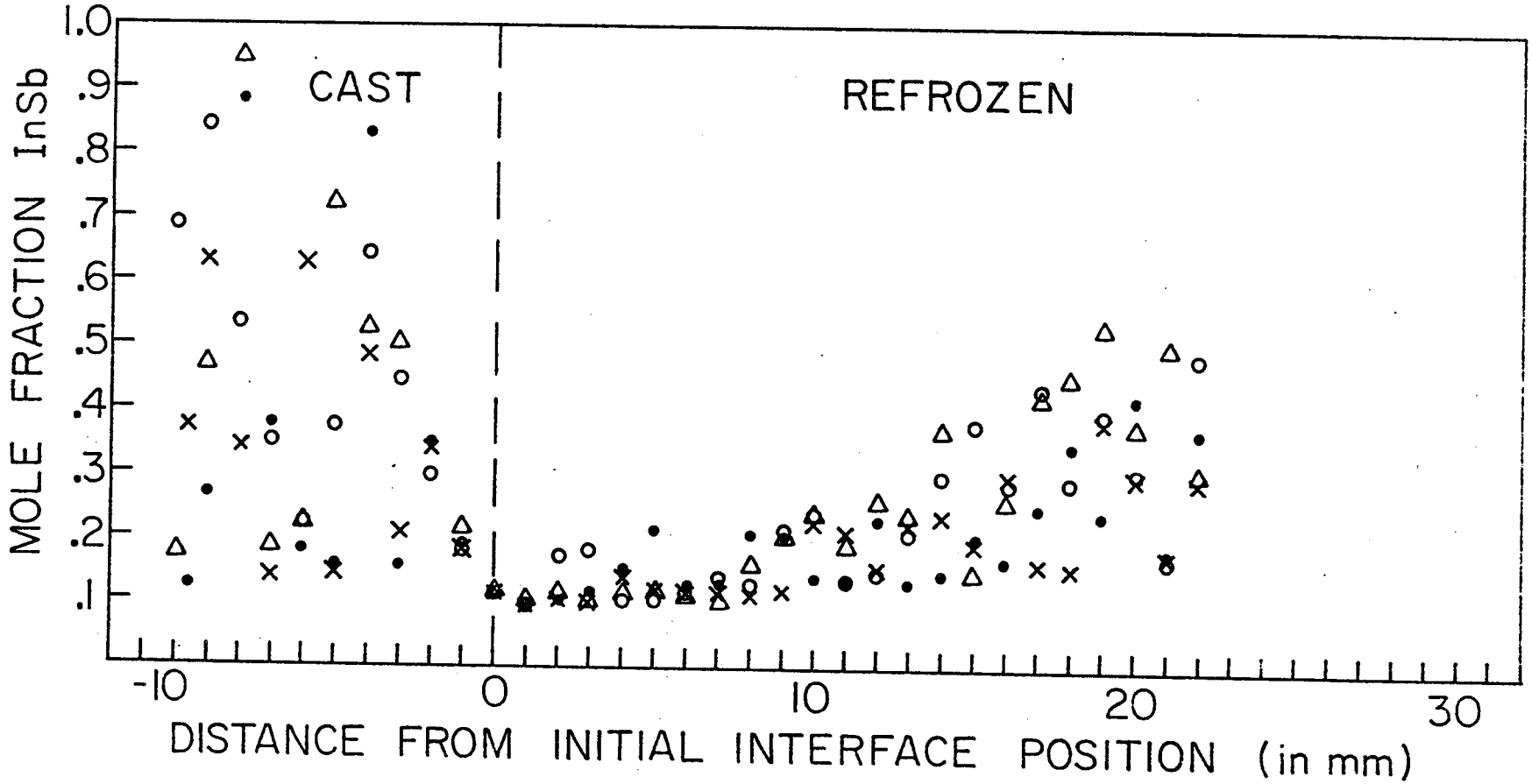

Figure 40. Electron microprobe results on NASA ingot 3A ($In_{0.5}Ga_{0.5}Sb$ processed horizontally).

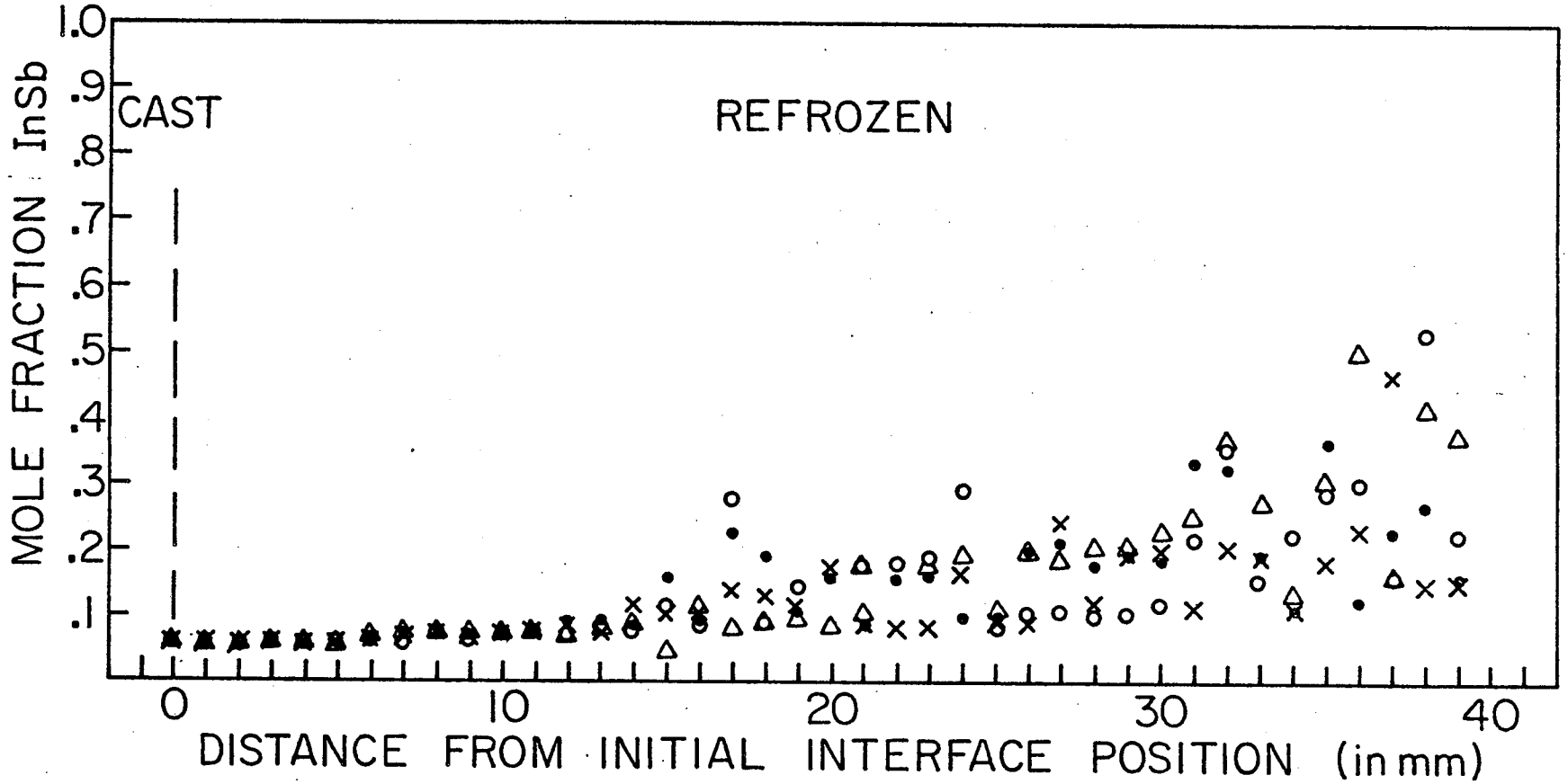

Figure 41. Electron microprobe results on NASA ingot 4B ($In_{0.3}Ga_{0.7}Sb$ processed horizontally).

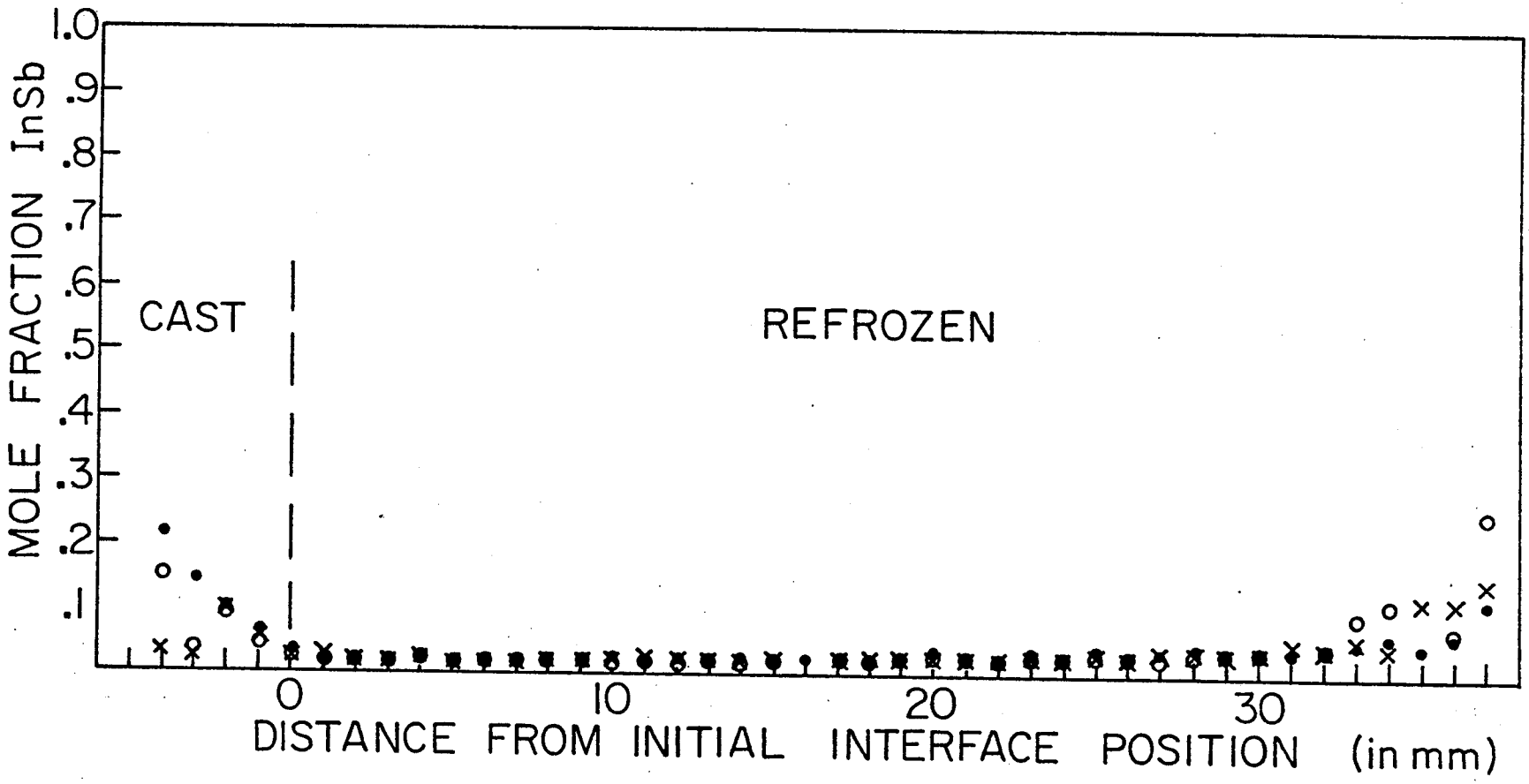

Figure 42. Electron microprobe results on NASA ingot 4C ($In_{0.1}Ga_{0.9}Sb$ processed horizontally).

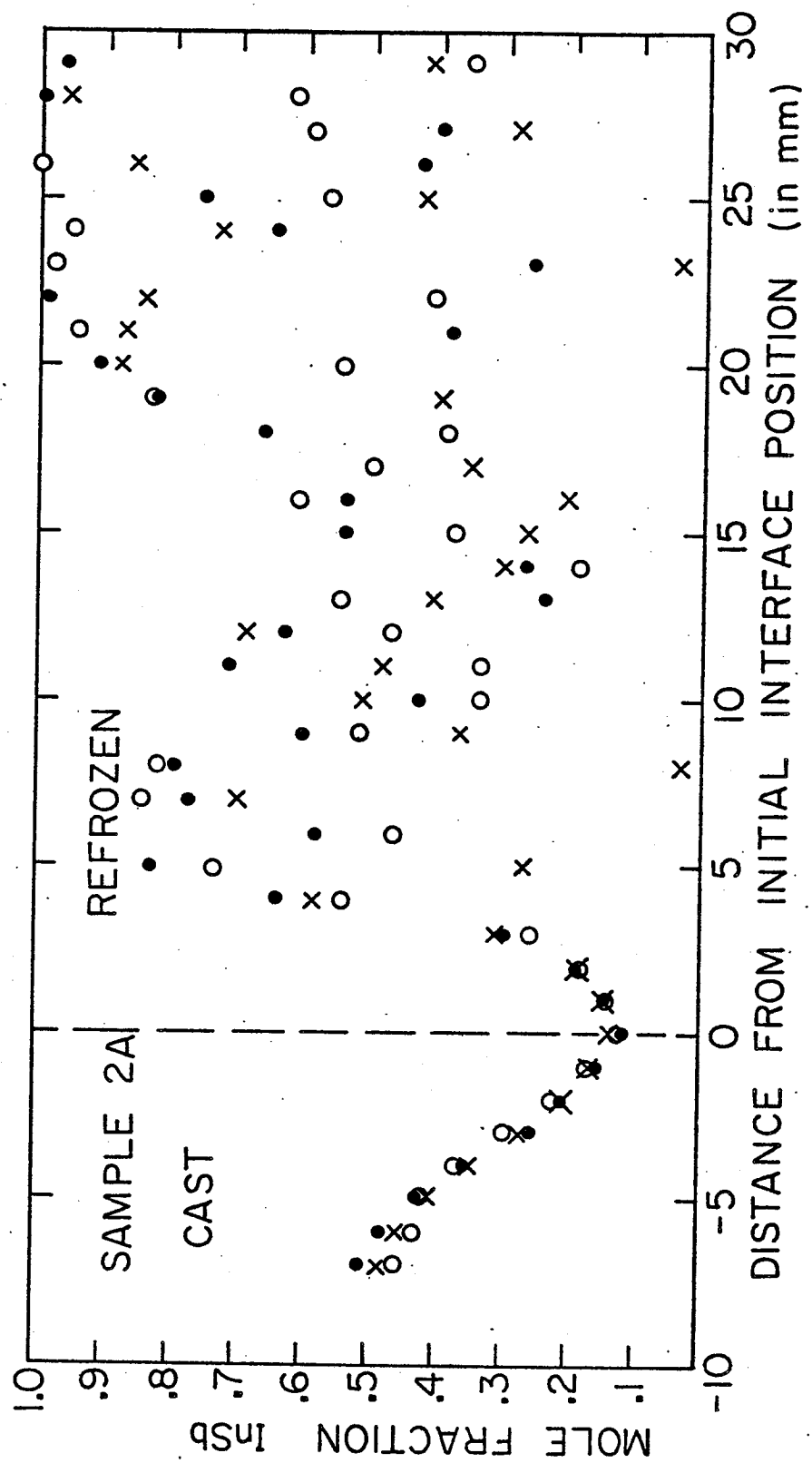

Figure 43. Electron microprobe results on NASA ingot 2A ($In_{0.5}Ga_{0.5}Sb$ processed in SL-3).

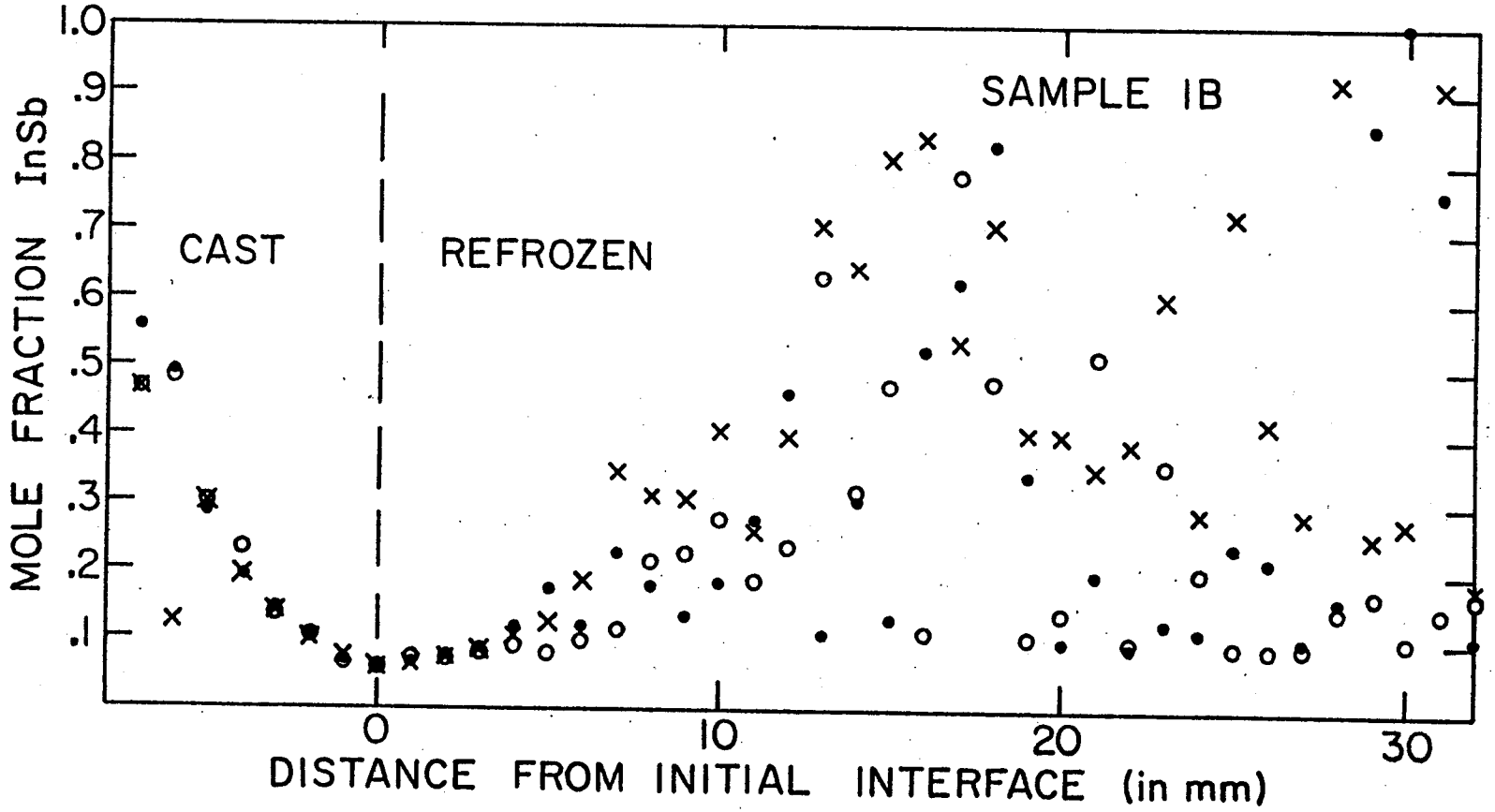

Figure 44. Electron microprobe results on NASA ingot 1B ($In_{0.3}Ga_{0.7}Sb$ processed in SL-3).

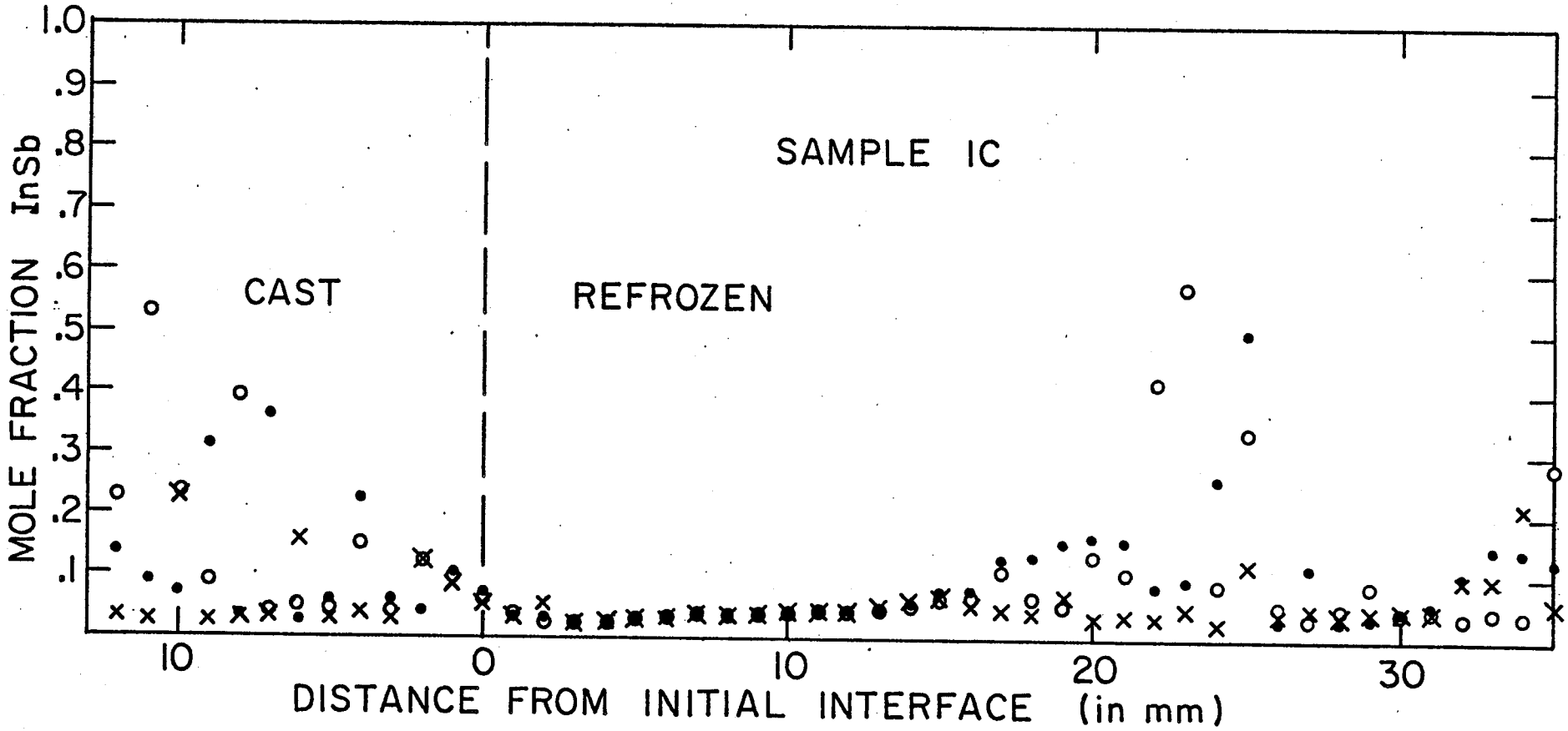

Figure 45. Electron microprobe results on NASA ingot 1C ($In_{0.1}Ga_{0.9}Sb$ processed in SL-3).

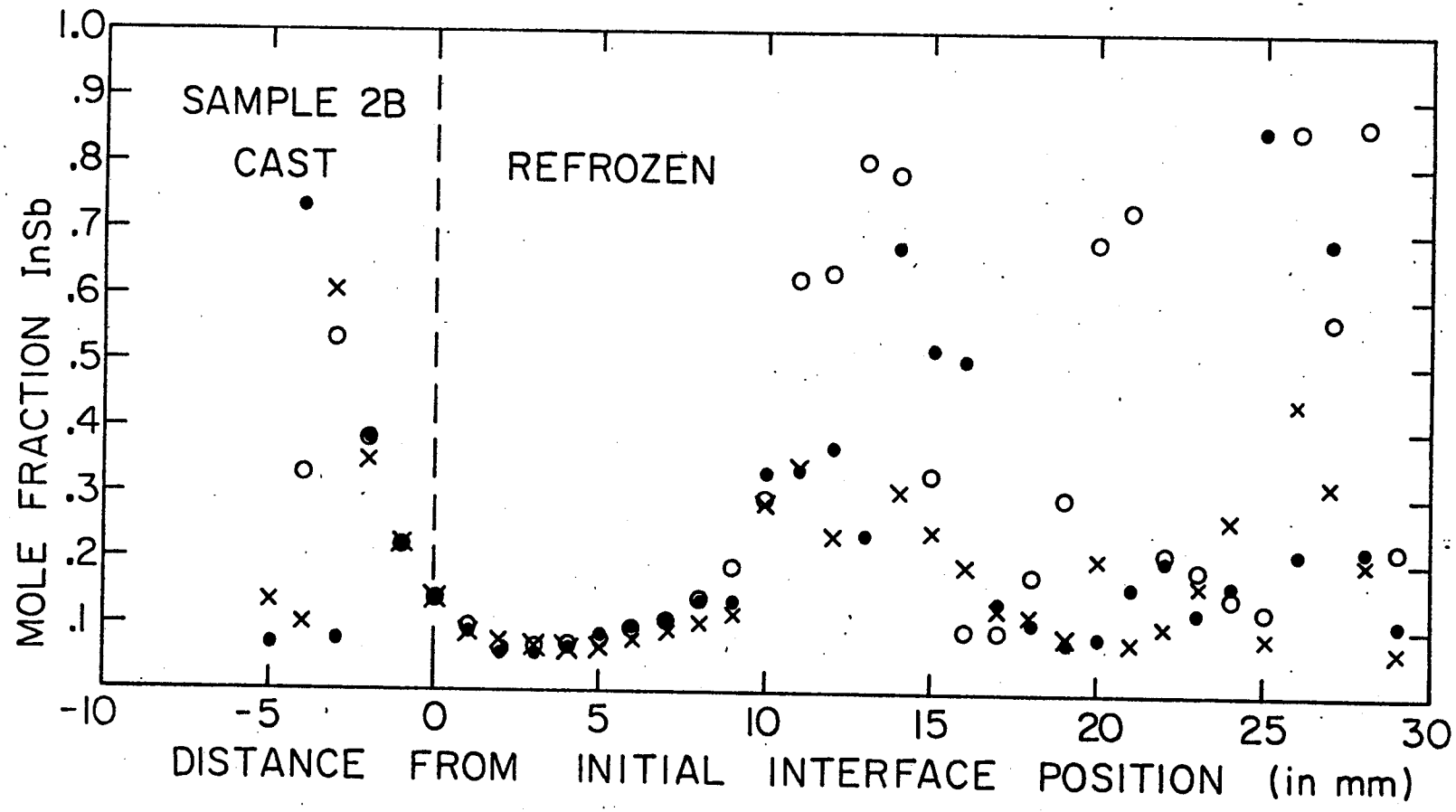

Figure 46. Electron microprobe results on NASA ingot 2B ($In_{0.3}Ga_{0.7}Sb$ processed in SL-4).

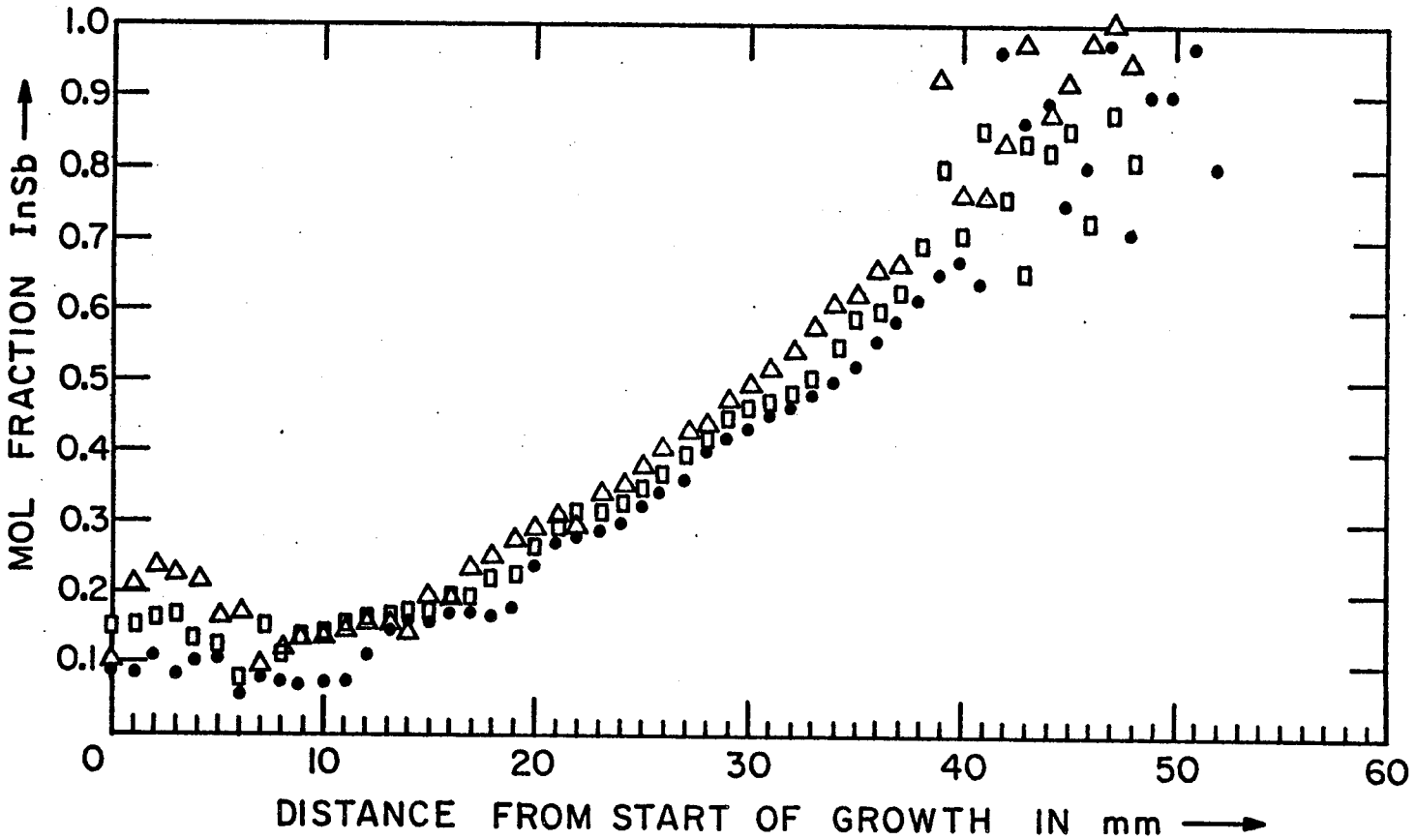

Figure 47. Electron microprobe results on USC ingot DF-9 (Bridgman-grown).

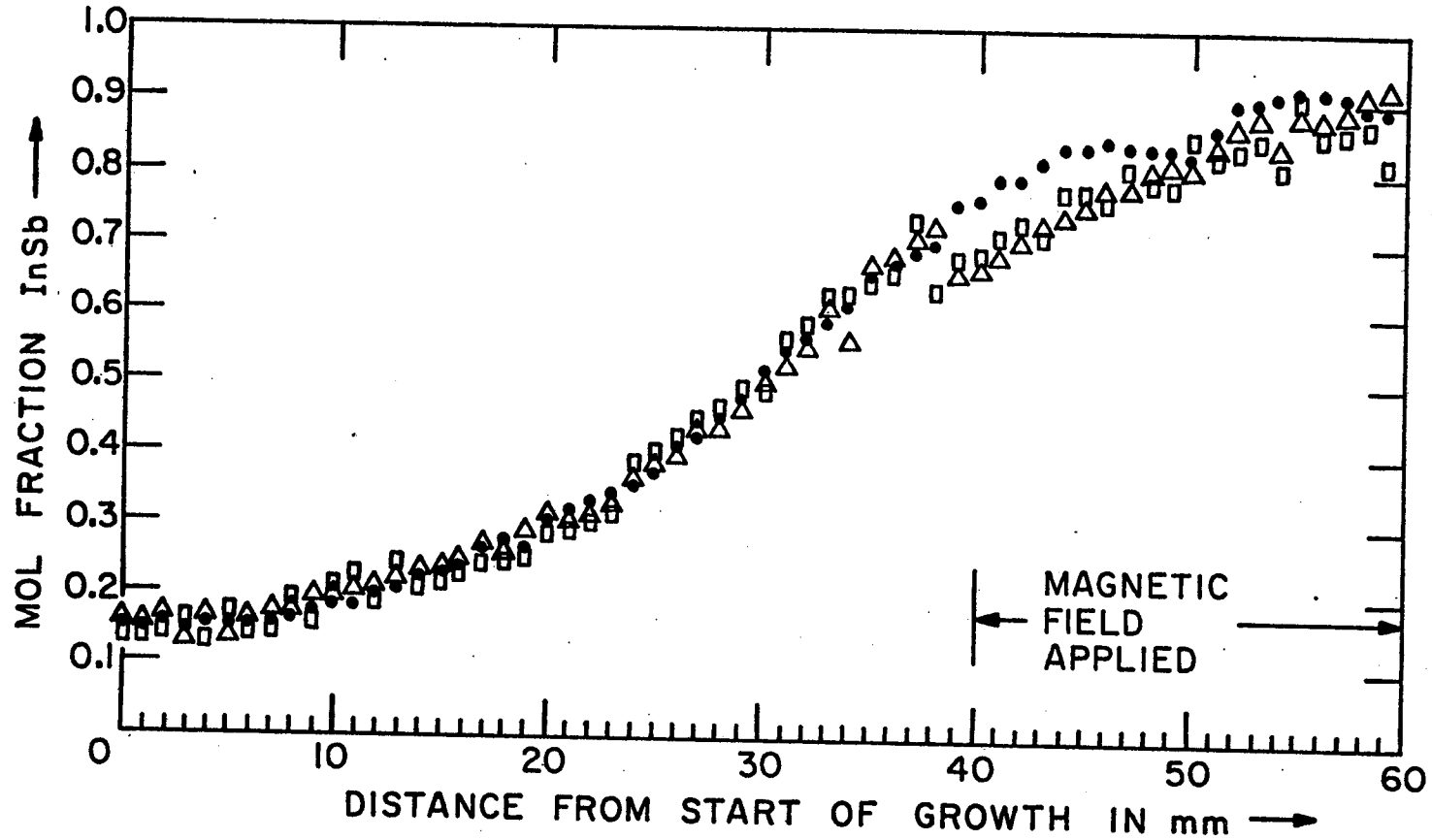

Figure 48. Electron microprobe results on USC ingot DF-11 (Bridgman-grown).

constitutional supercooling. From Figure 2, the tendency toward instability should increase as the In content of the melt at the interface increases, as the temperature gradient decreases, and as the freezing rate increases. All three of these trends occurred as solidification proceeded. Note, however, that a much longer length of stable growth was obtained with horizontal processing. There were two reasons for this, both related to free-convective stirring. The melt-back was greater with horizontal processing, as noted in Table I. This caused the interfacial temperature gradient to be larger since the distance from the interface to the heat sink was decreased. Secondly, the free convective stirring of the melt decreased the In concentration in the melt at the interface, which was also reflected in the difference in macroscopic concentration profiles, as noted earlier. Table III compares values of G/V from the Westinghouse heat transfer results (6) with those from Figure 2 for constitutional supercooling under the conditions at which the inhomogeneities began. The agreement is only fair.

The scanner on the electron microprobe was not operational so that possible micro-inhomogeneities could not be scanned in detail. An attempt was made to detect fluctuations in In concentration along the growth direction in the slow regrowth region of vertically-processed sample 2C near the initial interface by taking point counts two microns apart over a distance of twenty microns. No variation was detected. This means either that there was no variation or that this method was not sufficiently sensitive to detect it.

An attempt was also made to determine if gravity segregation occurred in the horizontally-grown sample 4C by taking point counts 0.4 mm apart across the width of the sample. If gravity segregation had occurred, there would have been a vertical compositional variation due to the combination of free convection and segregation at the growing interface. No variation was detected, probably because of the very slow growth rates.

TABLE III. VALUES OF G/V ESTIMATED AT POINTS AT WHICH INHOMOGENEITIES BECOME NOTICEABLE IN ELECTRON MICROPROBE RESULTS ON NASA INGOTS

Run	From Westinghouse Calculations[6]	From Figure 2 for Constitutional Supercooling with $D = 2 \times 10^{-5}$ cm^2/sec
	Vertical	
1A(c)	570	500
3B	670	1000
2C	570	500
	Horizontal	
3A	670	1200
4B	550	870
4C	330	400
	SL-3	
2A	800	1800
1B	670	1000
1C	550	500
	SL-4	
2B	710	1000

IV. CONCLUSIONS AND DISCUSSION

Several interesting effects of gravity were revealed by these experiments. The concentration profiles and the compositional homogeneity were both strongly influenced by the magnitude and direction of g, as expected from free convection effects. The lack of convective stirring in space-processing leads to a significant initial compositional transient which cannot be entirely avoided, although it can be greatly reduced by lowering the freezing rate. A lower freezing rate would also avoid compositional inhomogeneities due to constitutional supercooling. Production of a homogeneous ingot would probably eliminate cracking.

The most exciting development was the great reduction in twinning brought about by space processing. Since the cause of growth twinning is not really known, we can only speculate that foreign particles are responsible and that these interact more frequently with the growing interface when convection is present.

The ingots processed in SL-3 had a smaller diameter than the tube. Apparently the melt did not wet the carbon coating. Surface tension decreases with increasing temperature, and the temperature increased with distance from the interface down the melt. This would have forced the melt to contract near the interface and to expand at the hot end. Those processed in SL-4 had the same diameter as the tube. The only difference between these two runs was that the heater temperature was higher in SL-4. Since the compositions were the same, the interface temperatures were the same, although the portion of the melt in the heater would have been hotter in SL-4. We can only speculate that this higher temperature caused the melt to first wet the tube wall and then to spread down to the interface.

A wide variety of grain sizes was observed, but with no trend yet observed. Sadly, there appears to be no large advantage to space processing of alloys from this standpoint.

The preferred grain orientation was <111> in all cases.

We have no explanation for the great difficulty in distinguishing grains in the space-processed ingots.

Gas bubbles were more uniformly distributed in the space-processed ingots, but this is not significant since they can be avoided entirely by solidification in a reasonable vacuum (5).

Acknowledgments

The fabrication and characterization of the NASA samples was supported by NAS8-28305. The X-ray Laue patterns and the USC solidification experiments and characterization was supported by the Joint Services Electronics Program monitored by the Air Force Office of Scientific Research under Contract No. F44620-71-C-0067.

We are grateful to Vincent Yip for assisting with the fabrication of the NASA ampoules and to Jack Worrall for the electron microprobe work.

References

1. J. C. McGroddy, M. R. Lorenz and T. S. Plaskett, Solid State Commun., 7, 901 (1969).

2. G. M. Blom and T. S. Plaskett, J. Electrochem. Soc. 118, 1831 (1971).

3. W. R. Wilcox, J. Crystal Growth 12, 93 (1972).

4. H. P. Utech and M. C. Fleming, J. Appl. Phys. 37, 5 (1966).

5. W. R. Wilcox, J. Crystal Growth 19, 221 (1973).

6. R. G. Seidensticker and J. W. Chi, "Ground Base Test Report of the Multipurpose Electric Furnace System M-518", Westinghouse Report WANL TME 2838 (Pittsburgh, 1973), under Contract NAS8-28271.